Received: 6 June 2022 | Revised: 12 April 2023 | Accepted: 28 June 2023

DOI: 10.1002/qj.4520

Quarterly Journal of the Royal Meteorological Society RMetS

RESEARCH ARTICLE

An assessment of Arctic diurnal water-vapour cycles in Canada's weather forecast model and ERA5

Shannon Hicks-Jalali[1] | **Zen Mariani**[1] | **Barbara Casati**[2] | **Sylvie Leroyer**[2] | **François Lemay**[3] | **Robert W. Crawford**[1]

[1]Meteorological Research Division, Environment and Climate Change Canada, Toronto, Ontario, Canada

[2]Meteorological Research Division, Environment and Climate Change Canada, Dorval, Quebec, Canada

[3]Canadian Centre for Meteorological and Environmental Prediction, Environment and Climate Change Canada, Dorval, Quebec, Canada

Correspondence
Shannon Hicks-Jalali, Meteorological Research Division, Environment and Climate Change Canada, Toronto, Ontario, Canada.
Email: shannon.hicks-jalali@ec.gc.ca

Abstract

The diurnal water-vapour cycle is a critical component of the hydrological cycle, yet it is one of the hardest components to accurately reproduce in forecast and climate models. Previous studies have shown that both forecast and climate models underrepresent the diurnal water-vapour cycle, which leads to errors in precipitation, cloud, and radiative transfer parameters. Most diurnal cycle studies were conducted in the Tropics, and very few model evaluations of this process exist for the Arctic. Additionally, the majority of studies focus on total column water-vapour cycles; almost none use height-resolved measurements. In this study, we evaluate the diurnal water-vapour cycles in Environment and Climate Change Canada's Global Environmental Multiscale–High Resolution Deterministic Prediction System (GEM–HRDPS) numerical weather forecast model and the European Centre for Medium-Range Weather Forecasts Reanalysis v5 (ERA5) using a Vaisala preproduction differential absorption lidar (DIAL) and a co-located Global Positioning System (GPS) located in Iqaluit, Nunavut (63.75° N, 68.55° W). Both numerical products reproduce the phase of the diurnal cycle well below 1 km year-round. However, ERA5's diurnal amplitudes are significantly smaller than the DIAL and GPS amplitudes. GEM–HRDPS amplitudes are consistently larger in the first few hundred metres but smaller above 1 km; it also underrepresents the amplitude of the total column diurnal cycle. Neither ERA5 nor GEM–HRDPS accurately reproduce the 12-hr component of the diurnal cycle in either the height-resolved or total column cycles. The inability to accurately reproduce the 12-hr component in both numerical products suggests that the representation of some underlying process is incomplete, which can impact the accuracy of precipitation and radiative transfer algorithms. In conclusion, we find that the numerical products are able to reproduce the general behaviour and shape of the cycle but still require improvement at certain altitudes.

KEYWORDS

diurnal cycle, water vapour, lidar, GPS, arctic, reanalysis, NWP

This is an open access article under the terms of the Creative Commons Attribution-NonCommercial License, which permits use, distribution and reproduction in any medium, provided the original work is properly cited and is not used for commercial purposes.

© 2023 His Majesty the King in Right of Canada. Quarterly Journal of the Royal Meteorological Society published by John Wiley & Sons Ltd on behalf of Royal Meteorological Society. Reproduced with the permission of the Minister of Environment and Climate Change Canada.

1 | INTRODUCTION

The diurnal cycle of water vapour is one of the most critical components of the hydrological cycle. It is an integral component of convection, precipitation, and other physical processes in weather and climate numerical models. As such, it is an excellent diagnostic variable for model evaluation, since it encompasses and mirrors several aspects of model performance. The diurnal cycle has been, and largely still is, one of the most difficult components to reproduce in atmospheric numerical models (for climate and weather forecasting) (Dai and Trenberth, 2004; Bock *et al.,* 2007; Bechtold *et al.,* 2008).

Though climate and weather forecasting models can reproduce climatological, seasonal, subseasonal, and mesoscale processes quite well, the diurnal cycle remains a challenge. Typical problems have included convection starting too early during warm seasons by 2-4 hr, extended daytime convection over land, incorrect cloud type formation resulting in errors in radiation transfer, and low integrated water vapour (IWV) diurnal amplitudes (Dai and Trenberth, 2004; Bechtold *et al.,* 2008; Stratton and Stirling, 2012). For example, Bechtold *et al.* (2008) found that the early initiation of convection and extended convection throughout the day delayed the onset of convective precipitation in many regions, thereby resulting in the underrepresentation of extreme precipitation events and less precipitation than observed. Thus, key improvements to modelling the diurnal cycle of convection were made (e.g., (Stratton and Stirling, 2012; Bechtold *et al.,* 2014)), which has resulted in the improvement of the precipitation diurnal cycle across much of the globe, particularly in regions of deep convection and in midlatitudes over land. Improvements to the convection diurnal cycle have direct impacts on precipitation, cloud, and radiative diurnal cycles. Thus, we should also expect to observe improvements in the water-vapour diurnal cycle.

Accurately modelling the diurnal water-vapour cycle has been hampered by the lack of instrumentation and observations capable of resolving the diurnal scale. Radiosondes have been the instrument of choice for humidity profile measurements; however, as they are usually only launched twice per day, they cannot accurately resolve the diurnal component. Additionally, the humidity sensors are prone to internal diurnal cycles that must be corrected (Miloshevich *et al.,* 2009; Dirksen *et al.,* 2014). Bevis *et al.* (1992) demonstrated that Global Positioning System (GPS) satellites could be used to obtain total column water vapour or IWV measurements on the scale of minutes; thus, it became one of the choice instruments for detecting diurnal cycles. Bouma and Stoew (2001) presented some of the first measurements of the diurnal water-vapour cycle in the Baltic region and examined the peak-to-peak amplitude of the 24 hr cycle. Dai *et al.* (2002) presented IWV diurnal cycles using GPS receivers for North America and further found that the IWV diurnal cycle has two primary components: the 24 hr diurnal and 12 hr semidiurnal. Since then, GPS measurements have become the preferred technique for deriving IWV diurnal cycles (e.g., Bock *et al.,* 2007; Jakobson *et al.,* 2009; Galisteo *et al.,* 2011; Lees *et al.,* 2021). GPS receivers lack the ability to distinguish height-resolved cycles and thus cannot resolve how the process evolves with altitude. There remains a lack of height-resolved diurnal water-vapour cycle studies, particularly in the boundary layer, due to the continued lack of high-frequency boundary-layer profiling instruments. Satellite-based imagers have been used to study upper tropospheric humidity diurnal cycles (Chung *et al.,* 2013; Xue *et al.,* 2020), as have ground-based microwave radiometers for the stratosphere and mesosphere (Haefele *et al.,* 2008; Hocke *et al.,* 2017). Louf *et al.* (2015) and Wang *et al.* (2002) both used a novel microwave radiometer to measure diurnal mixing-ratio cycles in the first 4 km as well at 100 m vertical resolution in Africa and Oklahoma respectively. Finally, Chepfer *et al.* (2019) used satellite-based microwave radiometer measurements to get 1–4 km vertical resolution height-resolved diurnal relative humidity cycles from 900 hPa to 200 hPa in the Tropics.

Thus, the bulk of diurnal water-vapour cycle research has focused on the Tropics and midlatitudes, been limited to either total-column or upper tropospheric and mesospheric altitude ranges, and most studies have relied on relatively low vertical resolution observations. Though the Tropics make an excellent region for diurnal cycle comparisons, higher latitudes continue to lack comparison studies due to the difficulty in maintaining ground-based observations for sufficient time-scales. High frequency and metre-scale weather (vertically) occur in the boundary layer; therefore, higher vertical resolution measurements can help resolve boundary-layer processes. Higher vertical water-vapour measurements have also been identified as a priority variable by the World Meteorological Organization (WMO) to improve our understanding of boundary-layer processes and forecasting (World Meteorological Organization, 2016; Montmerle, 2020).

In this study, we address both the need for higher vertical resolution and higher latitude observations of water vapour profiles. In 2018, Environment and Climate Change Canada (ECCC) deployed a preproduction Vaisala lidar (Mariani *et al.,* 2020; Newsom *et al.,* 2020; Gaffard *et al.,* 2021; Mariani *et al.,* 2021) and installed it at the Iqaluit, Nunavut supersite (Joe *et al.,* 2020). The lidar is a differential absorption lidar (DIAL) capable of producing specific humidity profiles from 90 m to 3 km altitude above ground level (depending on the meteorological conditions)

1477870x, 0, Downloaded from https://rmets.onlinelibrary.wiley.com/doi/10.1002/qj.4520 by German Meteorological Service, Wiley Online Library on [06/08/2023]. See the Terms and Conditions (https://onlinelibrary.wiley.com/terms-and-conditions) on Wiley Online Library for rules of use; OA articles are governed by the applicable Creative Commons License

at 100–300 m vertical resolution (in the first 1.5 km altitude) at a temporal frequency of 20 min. Its high temporal and vertical resolution make it an ideal instrument for studying boundary-layer processes and the diurnal cycle. The Vaisala DIAL is also not assimilated into forecasting or climate models, and is therefore an ideal tool as an independent source for model verification.

Hicks-Jalali *et al.* (2021) presented the first height-resolved diurnal water-vapour cycles using lidar measurements in the Arctic. They showed that the diurnal water-vapour cycles measured by the DIAL agreed well with the co-located WMO surface station mixing ratio and temperature cycles, as well as with the co-located GPS IWV diurnal cycles. The DIAL results were also verified against available literature (Dai *et al.,* 2002; Jakobson *et al.,* 2009; Jakobson *et al.,* 2014) for Arctic diurnal water-vapour cycles. As such, in this follow-up study we use the Hicks-Jalali *et al.* (2021) results to evaluate the diurnal specific humidity and IWV cycles from the European Centre for Medium-Range Weather Forecasts Reanalysis v5 (ERA5; Hersbach *et al.* (2020)) and ECCC's Global Environment Multiscale (GEM)–High Resolution Deterministic Prediction System (HRDPS) numerical weather prediction (NWP) model Milbrandt *et al.* (2016). In this article we will refer to both ERA5 and GEM-HRDPS as "numerical products". Both numerical products have recently implemented new convection and microphysics schemes and have made updates to their assimilated observations. Additionally, the diurnal water-vapour cycles in GEM have never been evaluated for the Arctic. The goal of this study is to demonstrate the value in using lidar measurements for NWP validation, as well as to evaluate the numerical products' current diurnal water-vapour cycles to help guide future improvements.

The instrumentation, NWP model, and reanalysis used in this study, and the preparation of their measurements or output, are described in Section 2. Section 3 presents the method used to calculate the diurnal water-vapour cycle. The results and their discussion are in Sections 4 and 5 respectively. Finally, the summary and conclusions are presented in Section 6.

2 | DATA AND DATA PROCESSING

2.1 | Vaisala differential absorption lidar

The Vaisala DIAL is a preproduction water vapour broad-band lidar designed for operational meteorological measurements. DIALs are ideally suited for operational meteorology owing to their high temporal and vertical resolution in the boundary layer. The DIAL provides water vapour profiles from 90 m above ground level to approximately 3 km depending on the meteorological conditions. Unlike the Raman method, in which the return signal measured by the lidar is proportional to the Raman scattering of a single laser signal, the DIAL method uses the difference in atmospheric absorption between two laser signals. The difference in atmospheric absorption can be calculated by taking the ratio of the "online" (911.0 nm, water sensitive) and "offline" (910.6 nm, water insensitive) signals (P_{on}, P_{off}):

$$\frac{P_{\nu,\text{on}}}{P_{\nu,\text{off}}} \simeq \frac{\int_{-\infty}^{\infty} S_{\text{on}}(\nu-\nu_{\text{on}}) T_{\text{WV}}^2(\nu,z)\, d\nu}{\int_{-\infty}^{\infty} S_{\text{off}}(\nu-\nu_{\text{off}}) T_{\text{WV}}^2(\nu,z)\, d\nu}, \tag{1}$$

where $S_{\text{on,off}}$ is the normalized laser spectrum for each frequency ν, $T_{\text{WV}}(\nu,z)$. Equation (2) is the one-way atmospheric transmission due to water vapour absorption at each frequency with altitude z:

$$T_{\text{WV}}(\nu,z) = -\left(\exp \int_0^z N(z)\gamma(\nu,z)\, dz\right). \tag{2}$$

The water vapour transmission is a function of the water vapour number density $N(z)$ and the water vapour absorption cross-section $\gamma(\nu,z)$. The derivation of Equation (1) can be found in Newsom *et al.* (2020).

The DIAL uses an inverse method similar to that in South *et al.* (1998) to solve for the water vapour number density profile. The water vapour profiles are calculated with respect to ground level; however, for simplicity we just use "metres" to represent "metres above ground level". Note that the Iqaluit supersite is only approximately 10 m above sea level; therefore, metres above ground level and metres above sea level are almost the same. The water vapour mixing ratio profiles are then calculated using a weather sensor present on the DIAL and extrapolating the temperature and pressure profiles using the International Organization for Standardization (ISO) 2533:1975 standard atmospheric model with a vertical temperature gradient of $-0.0065\,\text{K}\cdot\text{m}^{-1}$. A more detailed description of the DIAL's retrieval algorithm can be found in Newsom *et al.* (2020). Updated parameters for the preproduction model retrieval and design are presented in tab. 2 of Hicks-Jalali *et al.* (2021) and Mariani *et al.* (2021).

The DIAL mixing ratio profiles have been evaluated over several validation campaigns in various climates and meteorological conditions. The initial prototype was presented in Newsom *et al.* (2020), which validated the prototype DIAL against radiosondes, a Raman water vapour lidar, and an atmospheric emitted radiance interferometer (Knuteson *et al.,* (2004a); Knuteson *et al.,* (2004b)) at the Great Plains Atmospheric Radiation Measurement research site in Oklahoma. They found that the DIAL was effectively unbiased against the radiosondes and the

1477870x, 0, Downloaded from https://rmets.onlinelibrary.wiley.com/doi/10.1002/qj.4520 by German Meteorological Service, Wiley Online Library on [06/08/2023]. See the Terms and Conditions (https://onlinelibrary.wiley.com/terms-and-conditions) on Wiley Online Library for rules of use; OA articles are governed by the applicable Creative Commons License

Raman lidar ($-0.01\,g{\cdot}kg^{-1}$), but had a slight dry bias of $-0.22\,g{\cdot}kg^{-1}$ against the atmospheric emitted radiance interferometer. ECCC deployed the new preproduction model in early 2018 and validated it against a Raman lidar at the ECCC site in Toronto (Mariani *et al.,* 2020). It was found to work well in urban conditions with a minimal overall bias of $0.17 \pm 0.14\,g{\cdot}kg^{-1}$. It was then validated a second time for Arctic conditions against coincident radiosondes and the Canadian autonomous Arctic aerosol lidar (a Raman lidar) over a year-long period. Mariani *et al.* (2021) found a small systematic wet bias in the DIAL with respect to the radiosonde ($0.13 \pm 0.01\,g{\cdot}kg^{-1}$) and the Canadian autonomous Arctic aerosol lidar ($0.18 \pm 0.02\,g{\cdot}kg^{-1}$). The wet bias between the two instruments is due to an overestimation of the laser spectral width in the DIAL's water vapour retrieval algorithm and will be corrected by Vaisala in future algorithm updates. In addition to the small systematic bias, Mariani *et al.* (2021) found a diurnal cycle in the water vapour retrieval; the current retrieval is sensitive to solar background noise in the overlap region between the low-altitude and high-altitude channels (250–450 m). This sensitivity will be resolved by Vaisala in future models. Consequently, we have removed this altitude region from our diurnal analysis. Most recently, Gaffard *et al.* (2021) conducted a 1 month validation of a second preproduction version at the UK Met Office testing site in Cardington. They found biases of similar range and magnitude to the previous studies.

The height-resolved diurnal analysis in this study uses the same profiles and data processing as in Hicks-Jalali *et al.* (2021). We use DIAL water-vapour mixing ratio profiles from September 2018 to June 2020. The DIAL has a temporal resolution of 20 min but produces a rolling average profile every minute. For the purposes of this study, we used one profile per hour at the start of the hour for consistency with both numerical products. The profile is an average of the 20 min prior to the hour mark; for example, the average of 2040–2100 UTC is the profile used for 2100 UTC. Though the DIAL reports measurements every 4.8 m, Newsom *et al.* (2020) calculated the vertical resolution to range from 100 to 300 m, increasing with altitude. We vertically average the mixing ratio profiles to 100 m for the entire profile, noting that above 1 km the vertical resolution increases to 200 m. Therefore, the bins above 1 km may have some correlation.

2.2 | GPS

The Iqaluit ground-based GPS receiver is managed by National Resources Canada and the International Global Navigation Satellite System Service (IGS). The station was installed in late 2009 and has been operating continuously since then with less than 2% downtime. The total column water vapour amount, or IWV, can be calculated by determining the amount a satellite signal is delayed when it is sent from the satellite to the ground receiver. Bevis *et al.* (1992), Bevis *et al.* (1994), Emardson *et al.* (1998), and Jones *et al.* (2020) provide detailed summaries on the GPS IWV retrieval. The National Geodetic Laboratory at the University of Nevada has recently reprocessed the IGS database with an updated IWV retrieval (Blewitt *et al.,* 2018). The new IGS product now provides an IWV calculation. Hicks-Jalali *et al.* (2021) validated the National Geodetic Laboratory IWV measurements for Iqaluit against the twice-daily radiosondes launched from the Iqaluit supersite. The radiosonde and GPS IWV average values were well within the standard deviation of their respective measurements for all seasons, with the exception of a 1 mm wet bias for the GPS in the winter months. The wet bias is likely due to the radiosonde humidity sensor's sensitivity to cold temperatures (Miloshevich *et al.,* 2009; Dirksen *et al.,* 2014). Regardless, a systematic bias has little impact on the diurnal cycle solutions as the diurnal cycle is a relative calculation.

This study uses the same GPS diurnal cycle analysis conducted in Hicks-Jalali *et al.* (2021) from September 2009 through December 2019. Hicks-Jalali *et al.* (2021) found a discontinuity in the diurnal GPS measurements at 0000 UTC/1900 h local solar time. The IGS GPS IWV solutions are calculated in 24 hr batches, with no correlation between each 24 hr period. Small errors in total zenith delay from the satellite can result in discontinuities at the 24 hr mark (Brockman, 2020), which are unavoidable. To mitigate their effect on the diurnal solutions, the GPS measurements are averaged to a temporal resolution of 1 hr and filtered as in Hicks-Jalali *et al.* (2021). For this study, the solutions are shifted to UTC to facilitate comparisons with the models. GPS zenith total delay (ZTD) measurements are assimilated into the GEM–HRDPS forecast model, but not ERA5. As IWV measurements are derived from ZTD, the GPS and GEM results are not entirely independent. However, the GPS results are used to complement the DIAL results and illustrate the degree to which the numerical products agree or disagree with both instruments. We find that the disagreement between numerical products and GPS is similar to the disagreement between numerical products and DIAL, which leads us to conclude that the GEM–HRDPS's dependence on the GPS results is minimal.

2.3 | GEM–HRDPS

The HRDPS is a high-resolution NWP forecasting model developed by ECCC (Milbrandt *et al.,* 2016) based on the

1477870x, 0, Downloaded from https://rmets.onlinelibrary.wiley.com/doi/10.1002/qj.4520 by German Meteorological Service, Wiley Online Library on [06/08/2023]. See the Terms and Conditions (https://onlinelibrary.wiley.com/terms-and-conditions) on Wiley Online Library for rules of use; OA articles are governed by the applicable Creative Commons License

GEM atmospheric model (Côté *et al.,* 1998). Its domain covers the northern portion of the United States and the majority of Canada and has a horizontal resolution of approximately 2.5 km, or roughly 0.0225° on its rotated grid. At Iqaluit, the grid resolution is 2.42 km. It uses 62 vertical levels, with an approximate resolution of 100 m in the first 2 km of altitude (with 11 levels gradually stretched). The kilometre-scale resolution of HRDPS was shown to improve forecasts of 1–2 days, particularly in cases of squall lines and convective storms. The system has been operational at the Meteorological Service of Canada since 2015, with regular updates. Of importance for the period used in this study, the predicted particle properties microphysics scheme (Morrison and Milbrandt, 2015; Milbrandt and Morrison, 2016; Milbrandt *et al.,* 2018) was introduced with minor subsequent modifications. GEM–HRDPS is run four times per day starting at 0000, 0600, 1200, and 1800 UTC for 48 hr. Finally, despite the fact that HRDPS falls into the convection-permitting model category, the Kain and Fritsch (Kain and Fritsch, 1990) convection parametrization scheme was introduced to HRDPS and reduced the bias of the precipitation diurnal cycle for summertime precipitation (Milbrandt *et al.,* 2016).

Initial conditions for HRDPS come from different sources. Hydrometeor fields are created from the previous run's first 6 hr (Milbrandt *et al.,* 2016). This allows the HRDPS to start a forecast with fully developed clouds and microphysics and additional spin-up time is not required. The Canadian Land Data Analysis System (Carrera *et al.* (2015)) is a 2.5 km coupled assimilation system that provides a soil and vegetation scheme with the mean surface temperature and soil moisture variables to drive the atmospheric components. The Canadian Land Data Analysis System assimilates observations such as snow depth, temperature, dew-point, soil moisture, snow albedo, precipitation, and several other snow parameters. The kilometre-scale assimilation of soil moisture and precipitation can be important for convection due to the increased ability to model moisture gradients (Milbrandt *et al.,* 2016). It is worth mentioning that detailed initialization of sea-ice cover and surface temperature is not provided in the region of Iqaluit but only in the south for the Gulf of St Lawrence.

The HRDPS is based on and is driven by the ECCC's lower resolution (10 km) Regional Deterministic Prediction System (RDPS) model for initialization of other variables and for the lateral boundary conditions. In addition to the standard synoptic and satellite measurements, the RDPS assimilates ground-based GPS measurements from the NOAA Global Systems Division GPS network every 2 hr (Macpherson *et al.,* 2008; Buehner *et al.,* 2015; Caron *et al.,* 2015). Details on the GPS assimilation procedure can be found in Macpherson *et al.* (2008). RDPS assimilates both the ZTD and the surface pressure measurements from each station, including the Iqaluit station. Assimilating ZTD from GPS improved the precipitation forecasts for certain regions and lead times (Buehner *et al.,* 2015). Hydrometeor recycling is also performed in RDPS (Buehner *et al.,* 2015).

We use GEM–HRDPS specific humidity and IWV variable output over the same time frame as the DIAL measurements (September 2018–June 2020). The GEM–HRDPS (henceforth just GEM) variables are retrieved on the model native grid and then interpolated (by using the nearest grid point) to the Iqaluit supersite's latitude and longitude. To minimize dependence from radiosondes, which are assimilated at 0000 and 1200 UTC, we chose to use the forecasts starting at 0600 UTC. Avoiding dependence on the GPS assimilation was not possible since the GPS measurements are assimilated for every forecast run. To further mitigate any artefact from spin-up, we start the time-series calculation from the sixth hour after the 0600 UTC initialization time (sixth hour "lead time"), such that the time series is calculated in a 24 hr window from 1200 UTC to 1200 UTC the following day. The DIAL, GPS, and ERA5 time series begin at the same time to avoid differences due to the end points of the series.

In addition to the specific humidity and IWV variables, we also use the geopotential height variable provided for each model level to linearly interpolate the GEM specific humidity profiles to a standard altitude grid. The standard grid is a 100 m resolution grid chosen to coincide with the DIAL altitude grid. The standard model pressure-level grid has a vertical resolution of 25 hPa in the first 2 km; therefore, interpolation error is minimal. Note that the IWV variable in GEM is not a prognostic variable but is derived (and then integrated) from the specific humidity profile. The IWV is provided as a standard output variable; therefore, we have not calculated it separately.

2.4 | ERA5

ERA5 is the most recent version of the European Centre for Medium-Range Weather Forecasts reanalysis models (Hersbach *et al.,* 2020). ERA5 profiles are provided on 37 standard pressure levels from 1,000 hPa up to 1 hPa with a vertical resolution of 25 hPa up to 100 hPa. ERA5's horizontal resolution was increased to 0.25° × 0.25° (approximately 28 km north–south and 13 km east–west at Iqaluit) and uses a four-dimensional variational data assimilation scheme with the IFS Cycle 41r2 forecast model. The assimilation system uses 12-hourly windows from 0900 to 2100 UTC and then 2100 to 0900 UTC the next day. ERA5's land and ocean components are coupled to the

1477870x, 0, Downloaded from https://rmets.onlinelibrary.wiley.com/doi/10.1002/qj.4520 by German Meteorological Service, Wiley Online Library on [06/08/2023]. See the Terms and Conditions (https://onlinelibrary.wiley.com/terms-and-conditions) on Wiley Online Library for rules of use; OA articles are governed by the applicable Creative Commons License

atmosphere. The technical details of the ERA5 physics and assimilation scheme are discussed thoroughly in Hersbach *et al.* (2020), in addition to a detailed list of the observations used in the assimilation scheme.

Since ERA5's release there have been several validations of the humidity diurnal cycles. Most studies have focused on the Tropics, where convection is the strongest and a clear diurnal cycle can be observed (Chepfer *et al.,* 2019; Xue *et al.,* 2020; Lees *et al.,* 2021). Xue *et al.* (2020) and Lees *et al.* (2021) conducted comparisons between ERA5 and IWV and upper tropospheric humidity respectively. They found that ERA5 exhibited some discrepancies between the model and observations with regard to the IWV diurnal cycle and upper tropsospheric humidity. The ERA5 model IWV diurnal cycle amplitudes were underestimated with respect to the local GPS observations, and ERA5 had difficulty capturing night-time maximums over the open ocean. Lees *et al.* (2021) observed that ERA5 underestimated the diurnal amplitude of upper tropospheric humidity.

In this study we use the hourly profile product on pressure levels (Hersbach *et al.,* 2018a) for the specific humidity and geopotential profiles and the single-level product for the IWV variable (Hersbach *et al.,* 2018b). The ERA5 diurnal cycles are calculated over the same time periods as the DIAL cycles. We use the grid point closest to the DIAL for comparison (63.5° N, 68.75° W). ERA5 specific-humidity profiles from the hourly product are used for the height-resolved cycles, whereas the IWV cycles use the total column water vapour ("tcwv") variable. The relatively coarse vertical resolution of ERA5 in the boundary layer corresponds roughly to an altitude resolution of 200 m. Hourly ERA5 geopotential profiles were used to interpolate the specific humidity measurements onto a standard altitude grid. The standard grid was defined to minimize interpolation error across the seasons and centred on the same bins as the DIAL and GEM altitude grids.

3 | THE DIURNAL CYCLE

A diurnal cycle can be calculated via two methods. The first is by fitting a sinusoid to a time series via least-squares fitting (e.g., Dai *et al.,* 2002; Dai and Trenberth, 2004; Galisteo *et al.,* 2011; Jakobson *et al.,* 2014). The second method is to use fast-Fourier transforms to determine the phase and amplitude of each harmonic or component in the cycle (Soden, 2000; Tian *et al.,* 2004; Hocke *et al.,* 2017). The second method either requires a continuous time series with no breaks, or constructing a "composite day". A composite day method is necessary when measurements of a specific location are inconsistently spaced (such as with satellite measurements). The time series in this study are sampled with high enough frequency that creating a composite day is not necessary. The first methodology enables direct comparisons with previous Arctic diurnal cycle work, such as Dai *et al.* (2002), Jakobson *et al.* (2014), and Hicks-Jalali *et al.* (2021). Hence, in this study we use the first method and follow the least-squares fitting procedure as in Dai *et al.* (2002). The diurnal cycle is represented as a sinusoidal function of the form

$$I(t') = I_0 + \sum_{n=1}^{4} S_n(t') + R, \tag{3}$$

$$S_n(t') = a_n \cos(nt') + b_n \sin(nt'). \tag{4}$$

The water vapour time series I_t is the summation of the daily average I_0, residuals R, and the diurnal cycle components $S_n(t')$. Dai *et al.* (2002) found that two major components were present in their IWV time series across North America, and subsequent studies have corroborated their results. Hicks-Jalali *et al.* (2021) also found that the third and fourth harmonics in the cycle were negligible at Iqaluit. Therefore, $n = 1, 2$, where S_1 is the 24-hr component and S_2 is the 12-hr component. The amplitude A_n and phase ϕ_n for each harmonic are found via a_n and b_n, using the following relationships:

$$A_n = \sqrt{a_n^2 + b_n^2}, \tag{5}$$

$$\phi_n = \tan^{-1}\left(\frac{a_n}{b_n}\right). \tag{6}$$

All diurnal cycles presented here are relative diurnal cycles, or diurnal anomalies, where I_0 has been subtracted from the cycle. Subtracting the average removes any systematic biases between the models and the observations, highlighting the diurnal behaviour.

4 | RESULTS

As Iqaluit is relatively far north, we did not use conventional seasonal definitions. We follow the same seasonal definitions as described in Hicks-Jalali *et al.* (2021), where summer is April–August (AMJJA), fall is in September through October (SO), winter is November through January (NDJ), and the spring is February and March (FM). These seasons correspond to the amount of short-wave radiation received at Iqaluit throughout the year, which directly influences the corresponding water-vapour cycle (Semmler *et al.,* 2005).

1477870x, 0, Downloaded from https://rmets.onlinelibrary.wiley.com/doi/10.1002/qj.4520 by German Meteorological Service, Wiley Online Library on [06/08/2023]. See the Terms and Conditions (https://onlinelibrary.wiley.com/terms-and-conditions) on Wiley Online Library for rules of use; OA articles are governed by the applicable Creative Commons License

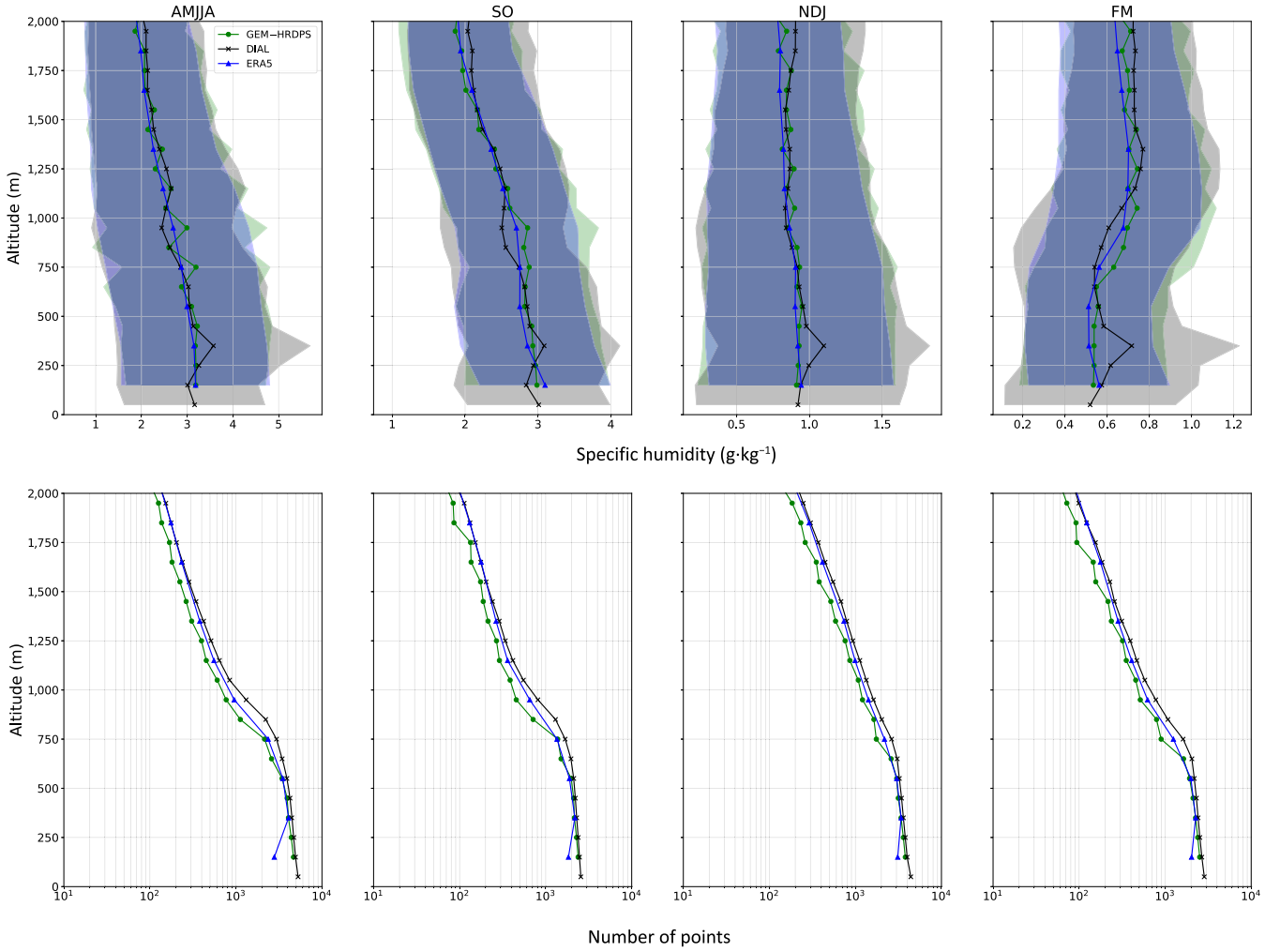

FIGURE 1 The average seasonal water vapour content at Iqaluit, Nunavut. Top: Seasonal averages of specific humidity and their standard deviation (shaded regions). Bottom: The number of hourly profiles used to calculate each average. Differential absorption lidar (DIAL, black ×), Global Environmental Multiscale–High Resolution Deterministic Prediction System (GEM–HRDPS, green dots), and European Centre for Medium-Range Weather Forecasts Reanalysis v5 (ERA5, blue triangles) profiles are shown. AMJJA: April–August; SO: September–October; NDJ: November–January; FM: February–March [Colour figure can be viewed at wileyonlinelibrary.com]

4.1 | Seasonal comparisons

The seasonally averaged water vapour profiles for ERA5, the DIAL, and GEM are presented in Figure 1 to provide environmental context and an evaluation of the models on a seasonal scale. Seasonal averages are equivalent to $I_0(z)$, Equation (3). ERA5 and GEM individual hourly profiles are limited to the same altitude range as the DIAL before averaging and then linearly interpolated to a standard altitude grid of 100 m for GEM and 200 m resolution for ERA5. Note that the spike between 250 and 350 m in the DIAL average is due to the interference from the solar background in the overlap region between the low-altitude channel and the high-altitude channel (Mariani *et al.*, 2021). Both models agree well with the DIAL and are within the standard deviation of each-other's measurements for all seasons. There are small biases between the models and the DIAL; however, they are all well within the 1σ variation of the water vapour over each season. Above 2 km there are not enough measurements to accurately calculate an average; therefore, we have removed these data from the analysis.

Summer and fall exhibit similar average profiles of 2.0–3.0 $g \cdot kg^{-1}$ due to the summer profile including the transition months (April and May) and a lag in water vapour concentration decrease from August to September. The standard deviation of the measurements decreases with altitude from approximately 1.0 $g \cdot kg^{-1}$ at the surface to 0.8 $g \cdot kg^{-1}$ at 1,800 m. During both seasons, there is a slight dry bias in the DIAL with respect to the numerical products of 0.25 $g \cdot kg^{-1}$ between 850 m and 1050 m, possibly due to the rapid drop in coincident measurements. In the summer above 1100 m, the DIAL is wet by 0.25 $g \cdot kg^{-1}$ with respect to both numerical products. This is a known

1477870x, 0, Downloaded from https://rmets.onlinelibrary.wiley.com/doi/10.1002/qj.4520 by German Meteorological Service, Wiley Online Library on [06/08/2023]. See the Terms and Conditions (https://onlinelibrary.wiley.com/terms-and-conditions) on Wiley Online Library for rules of use; OA articles are governed by the applicable Creative Commons License

TABLE 1 Seasonal averages of water vapour concentrations (in millimetres) for European Centre for Medium-Range Weather Forecasts Reanalysis v5 (ERA5), Global Environmental Multiscale–High Resolution Deterministic Prediction System (GEM–HRDPS), and Global Positioning System (GPS) integrated water vapour (IWV). Averages are presented as the mean plus/minus standard deviation of the IWV.

	IWV seasonal average $\pm SD$ (mm)			
Model	**Summer**	**Fall**	**Winter**	**Spring**
ERA5	10.48 ± 5.50	8.57 ± 3.84	3.02 ± 2.01	2.14 ± 1.01
GEM–HRDPS	10.93 ± 5.80	8.94 ± 4.03	3.43 ± 2.18	2.23 ± 1.14
GPS	10.84 ± 5.20	8.98 ± 3.72	4.36 ± 1.65	3.75 ± 0.82

issue, due to an incorrect assumption in the spectral width of the laser, which produces a systematic wet bias of approximately 0.2 g·kg^{-1} (Mariani *et al.,* 2021). The wet bias appears higher in altitude in the fall at 1,750 m.

Water vapour concentrations drop significantly in the winter to 0.8–0.9 g·kg^{-1}, with standard deviations between 0.7 and 0.3 g·kg^{-1} (decreasing with altitude). Similar to summer and fall, ERA5 is drier than the DIAL by approximately 0.1–0.2 g·kg^{-1} above 1 km. In the winter, GEM shows no dry bias relative to the DIAL until 1,750 m and has a smaller bias than ERA5 in the spring. Both numerical products are dry by 0.05 g·kg^{-1} with respect to the DIAL in the first 500 m in winter and spring.

ERA5 and GEM have excellent agreement with the GPS IWV measurements in summer and fall (Table 1). In the summer, the GPS measures a seasonal average of 10.84 mm and the ERA5 and GEM averages are within −0.44 mm and +0.09 mm respectively. All datasets had a standard deviation around 5 mm. The standard deviation is largest in the summer because April and May have smaller water vapour values than June through August, thereby increasing the variability over the entire season. In the fall, ERA5 again has a small dry bias with respect to the GPS of −0.41 mm, whereas GEM has almost no bias at −0.04 g·kg^{-1}. ERA5 has a dry bias with respect to the DIAL between 250 to 800 m (Figure 1), which is likely the cause for the dry bias in IWV as GEM has no dry bias in that region and almost no bias in IWV. Both models and the GPS have standard deviations on the order of 4 mm.

In the winter and spring, both models have around a 1 mm dry bias with respect to the GPS. Hicks-Jalali *et al.* (2021) found that in the winter months the radiosondes launched from Iqaluit have a similar dry bias with respect to the GPS, and radiosondes are known to have a dry bias at colder temperatures (Miloshevich *et al.,* 2009; Dirksen *et al.,* 2014). It is likely that the dry bias in the radiosondes affects the numerical products, as radiosondes are one of the primary data sources assimilated for their humidity profiles. Though we attempt to mitigate the affect of the radiosonde in the GEM results by choosing a lead time where they are not assimilated, there is some memory in the model that may contribute; this is explored in more detail in Section 4.4.

4.2 | Height-resolved diurnal cycles

The height-resolved diurnal cycles were calculated by fitting Equation (3) to the DIAL, ERA5, and GEM time series for each altitude bin and season. The amplitude and phase of each solution was then calculated using Equation (5) and Equation (6) respectively. Figure 2 shows the total diurnal cycle ($S_1 + S_2$) for each model and the DIAL, as well as the R^2 values for each fit as a function of altitude. Since the daily average $I_0(z)$ has been subtracted from the fit, this figure provides the relative change in the water vapour concentration. Using relative cycles removes the systematic biases discussed in Section 4.1. The grey/masked region in the DIAL solutions represents the region where there is a known internal instrumental diurnal cycle (Mariani *et al.,* 2020; Mariani *et al.,* 2021); therefore, we do not discuss the results from these altitudes. The time axis starts at 1200 UTC due to the GEM cycle time series starting at the 0600 UTC + 6 hr of lead time afterwards (1200 UTC). The DIAL and ERA5 cycles were also calculated starting at 1200 UTC to eliminate any possible discrepancy due to starting the diurnal fit at different times. Note that Iqaluit is located at UTC−0500.

For all seasons, DIAL amplitudes corresponding to lower R^2 values (generally above 1 km) must be treated with caution. Though some of the decrease in the fit may be due to random effects in the time series, comparisons with Jakobson *et al.* (2014) demonstrated that the summer cycle amplitudes and phases above 1 km (as below 1 km) are representative for the DIAL's latitude (Hicks-Jalali *et al.,* 2021), increasing confidence in these observations despite their lower R^2 values.

As Iqaluit is still below the Arctic Circle (66° 33′48.9″), there are still 3 hr of twilight around the summer solstice and around 6–10 hr of twilight and night-time in April, May, and August. Therefore, a clear diurnal cycle is visible in both models and the DIAL during the summer. The DIAL observes a peak in water vapour occurring at 2000 UTC (1500 h local time) in the first few hundred metres that then shifts to 25/0100 UTC above 600 m altitude as it is transported vertically. ERA5 and GEM also reproduce maximums around 2000 UTC in the first few hundred metres, which then gradually shift to later hours at higher altitudes. GEM reproduces larger maxima than the DIAL in the first few hundred meters by between 0.05

1477870x, 0, Downloaded from https://rmets.onlinelibrary.wiley.com/doi/10.1002/qj.4520 by German Meteorological Service, Wiley Online Library on [06/08/2023]. See the Terms and Conditions (https://onlinelibrary.wiley.com/terms-and-conditions) on Wiley Online Library for rules of use; OA articles are governed by the applicable Creative Commons License

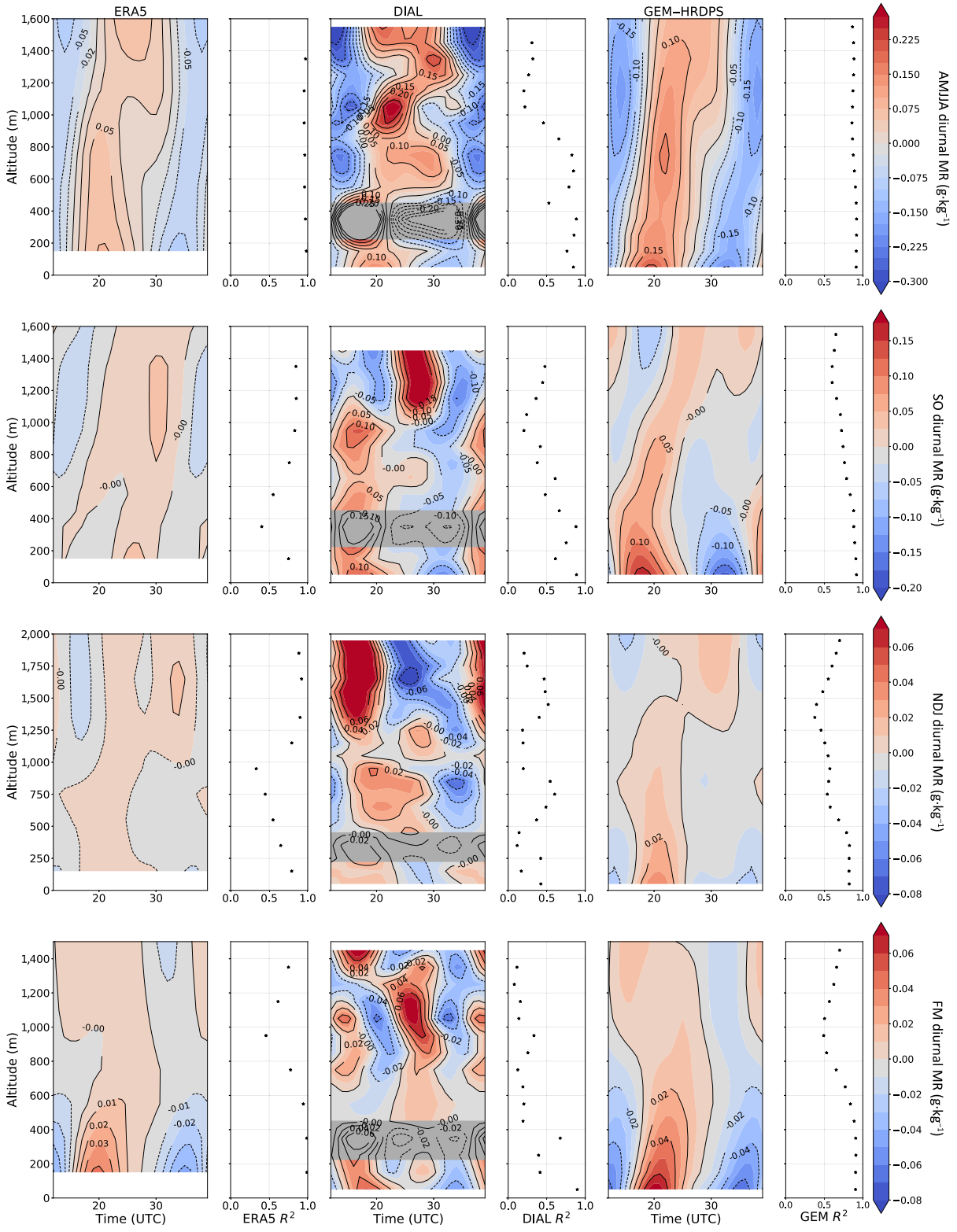

FIGURE 2 Diurnal water-vapour cycle solutions and accompanying R^2 values for the European Centre for Medium-Range Weather Forecasts Reanalysis v5 (ERA5; column 1), differential absorption lidar (DIAL; column 2), and Global Environmental Multiscale–High Resolution Deterministic Prediction System (GEM–HRDPS; column 3) for each season. Red colours (solid contours) represent increasing water-vapour mixing ratios (MRs) and blue colours (dashed contours) represent decreasing water-vapour MRs. Summer cycles (April–August, AMJJA) are shown in row 1, fall (September–October, SO) in row 2, winter (November–January, NDJ) in row 3, and spring (February–March, FM) in row 4. The daily average water vapour profile $I_0(z)$ has been subtracted from each solution to show the relative change in the MR (or diurnal anomaly). The DIAL's grey region between 250 and 450 m corresponds to the region of unreliable fits due to the known instrumental diurnal cycle and should be treated with caution. [Colour figure can be viewed at wileyonlinelibrary.com]

1477870x, 0, Downloaded from https://rmets.onlinelibrary.wiley.com/doi/10.1002/qj.4520 by German Meteorological Service, Wiley Online Library on [06/08/2023]. See the Terms and Conditions (https://onlinelibrary.wiley.com/terms-and-conditions) on Wiley Online Library for rules of use; OA articles are governed by the applicable Creative Commons License

and 0.08 g·kg^{-1}. GEM is able to reproduce the increase in amplitude that the DIAL observes at 700 m of 0.15 g·kg^{-1}; however, it does not reproduce the increase in amplitude above 1 km. Although ERA5 reproduces the overall phase of the cycle, its amplitudes are generally smaller by 0.1 g·kg^{-1} for all altitudes, with larger biases above 1 km.

The maximum of the DIAL diurnal cycle shifts to earlier in the day for the fall cycles for the first kilometre from the surface, with similar amplitudes as the summer. At 1 km there is an abrupt shift in the maximum's phase to 28/0400 UTC and a large increase in amplitude up to 0.2 g·kg^{-1}. ERA5 is not able to reproduce the fall cycle with the correct phase or magnitude until above 1 km. It has a maximum of 0.05 g·kg^{-1} at 0000 UTC, almost out of phase with the DIAL. GEM is able to reproduce a diurnal cycle that agrees with the first 800 m of the DIAL observations, albeit with a slightly larger amplitude of 0.15 g·kg^{-1}. However, whereas the DIAL observes an abrupt shift in phase at 1 km, the GEM maximum gradually shifts with altitude to 0000 UTC at 1,400 m. At 1,400 m the DIAL and GEM have maxima occurring at 1600–1700 UTC.

We note that numerical products tend to represent a smoother vertical transition of the diurnal cycle than the DIAL (in all seasons). This is expected due to their coarser resolution and need to preserve physical coherence/numerical stability through vertical levels. The abrupt shift at 1,000–1,200 m in the DIAL vertical profile of the diurnal cycle in the fall is possibly associated with the shift from the boundary layer to free troposphere (Hicks-Jalali *et al.*, 2021). This physically driven shift is, however, difficult to be depicted by the DIAL diurnal cycle fit (as shown by lower values of the goodness-of-fit measure, R^2), given its variability (e.g., in altitude) during transition seasons (such as fall). Overall more noisy data, with less performing fit, are expected from the DIAL (or any observation source) than in numerical products, but still they might better reflect real physical phenomena.

The winter and spring are extremely dry in Iqaluit, making the diurnal cycles difficult to resolve and thus creating low R^2 values, particularly for the DIAL. Similar to the fall, the winter maxima below 200 m for both models and the DIAL occurs around 1800 UTC. The time of the maximum stays relatively constant with altitude, with the exception of a slight shift to 2000 UTC between 400 and 1,250 m. Amplitudes are generally low, with a maximum of 0.02 g·kg^{-1} up to 1,250 m, where the DIAL observes a marked increase in amplitude up to 0.08 g·kg^{-1}. There is almost no diurnal cycle present in ERA5, which is also 12 hr out of phase with respect to the DIAL above 1 km. GEM produces a slightly larger diurnal cycle than ERA5 and is slightly more in phase with the DIAL (in the first kilometre). GEM's maxima in the first 200 m are also larger than the DIAL's by 0.02 g·kg^{-1}. GEM produces an increase in amplitude above 1 km similar to the DIAL; however, GEM and ERA5 phases are shifted by 12 hr (with respect to the DIAL) at that altitude.

As the amount of daylight increases in the spring, the DIAL's lower-altitude maximum increases to 0.05 g·kg^{-1} and shifts to later in the day closer to 1900 UTC. However, above 400 m the DIAL observes a later maximum at 0000 UTC, with a second maximum appearing at 1700 UTC above 600 m. The more complicated structure in the cycle is due to the shift in phase of the S_2 component (as will be shown). ERA5 and GEM's cycle are shifted later by 2 hr compared with the DIAL near the surface, and neither model agrees with the DIAL's cycle above 500 m (both for phase and amplitude). Whereas ERA5's cycle is of comparable amplitude to the DIAL between 150 and 300 m, GEM's amplitude is 40% more than that of the DIAL's.

Figures 3 and 4 separate the total diurnal cycle into their S_1 and S_2 components to further understand the behaviour of the total cycle. Figure 3 shows the amplitudes of the S_1 (row 1) and S_2 (row 2) components of ERA5, the DIAL, and GEM for each season, and Figure 4 provides the phases. The shaded region around each amplitude and phase profile is the standard deviation of the amplitude and phase solutions. The standard deviation is calculated by shifting the starting point of the time series from 0000 UTC to 2400 UTC to provide a distribution of solutions and examine the stability of the solutions. For ERA5 and the DIAL, this represents the sensitivity of the solutions to the edges of the time series. For GEM, it represents the stability of the solution with forecast lead time. We will discuss the standard deviations for GEM in more detail in Section 4.4.

The DIAL exhibits a clear correlation between amplitude and the seasonal cycle in the S_1 component, with the largest amplitudes in the summer (0.15–0.25 g·kg^{-1}) and smallest in the winter (0.02–0.1 g·kg^{-1}). The exception being between 450 m and 1 km, where the spring amplitudes are smaller than the winter amplitudes. The DIAL S_2 component exhibits a weaker correlation with the solar cycle, although the summer and fall cycle amplitudes are generally larger than the winter and spring cycles above 500 m, and the winter cycle has the lowest amplitudes for most altitudes. The S_2 amplitudes are smaller than the S_1 amplitudes. The DIAL amplitudes in both S_1 and S_2 components increase gradually with altitude, with the S_2 increasing faster than the S_1. The standard deviations of the DIAL amplitudes are small for all altitudes and seasons; therefore, the DIAL solutions are stable in amplitude.

Unlike the DIAL, ERA5 and GEM's amplitudes do not increase with altitude and are instead fairly constant or exhibit a decrease with altitude (e.g., for GEM's S_1 amplitudes, for fall winter and spring). GEM's S_1 amplitudes

1477870x, 0, Downloaded from https://rmets.onlinelibrary.wiley.com/doi/10.1002/qj.4520 by German Meteorological Service, Wiley Online Library on [06/08/2023]. See the Terms and Conditions (https://onlinelibrary.wiley.com/terms-and-conditions) on Wiley Online Library for rules of use; OA articles are governed by the applicable Creative Commons License

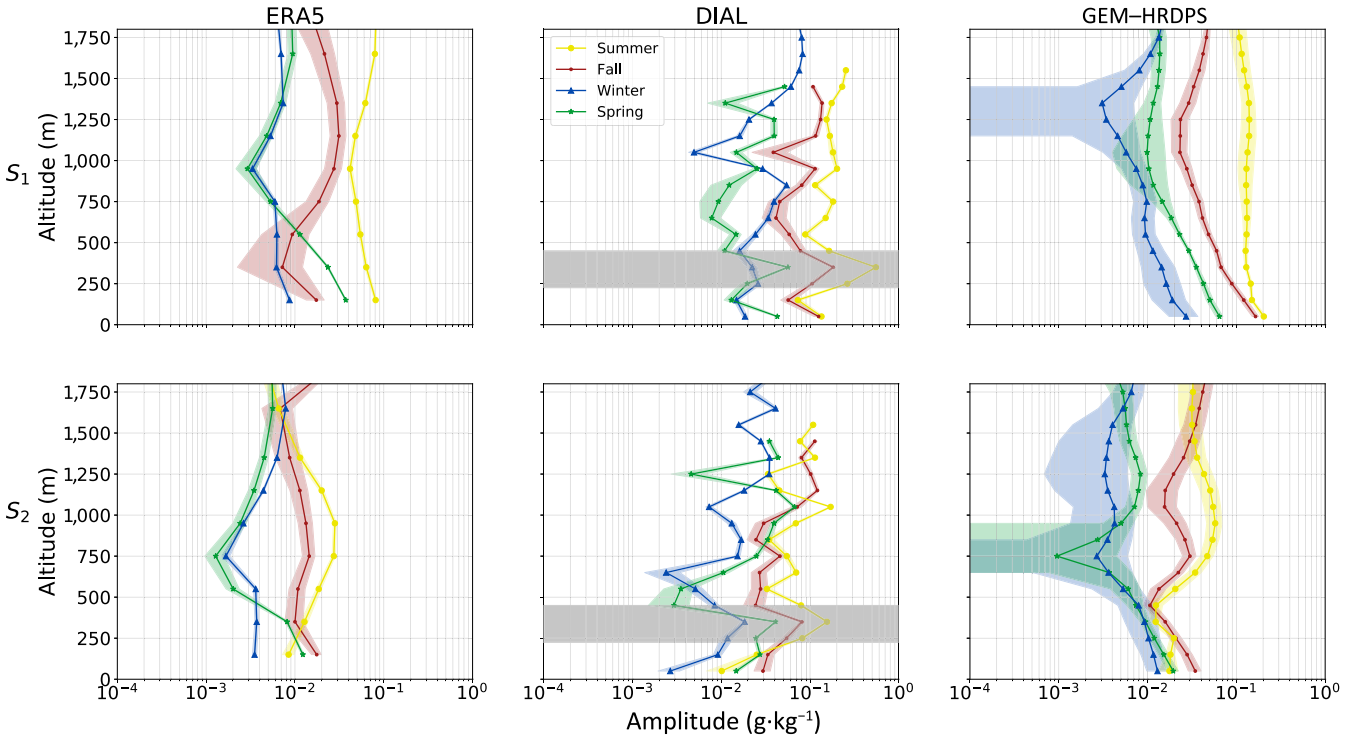

FIGURE 3 Diurnal water-vapour mixing ratio cycle amplitudes for European Centre for Medium-Range Weather Forecasts Reanalysis v5 (ERA5; column 1), differential absorption lidar (DIAL; column 2), and Global Environmental Multiscale–High Resolution Deterministic Prediction System (GEM-HRDPS; column 3). Rows 1 and 2 are the S_1 and S_2 amplitudes respectively. Similar to Figure 2, the greyed region represents the altitudes where there is an instrumental diurnal cycle and the DIAL fits are treated with caution. Summer (April–August, yellow circles), fall (September–October, red dots), winter (November–January, blue triangles), and spring (February–March, green stars) are shown. The standard deviation of the amplitude is the shaded region around each profile. [Colour figure can be viewed at wileyonlinelibrary.com]

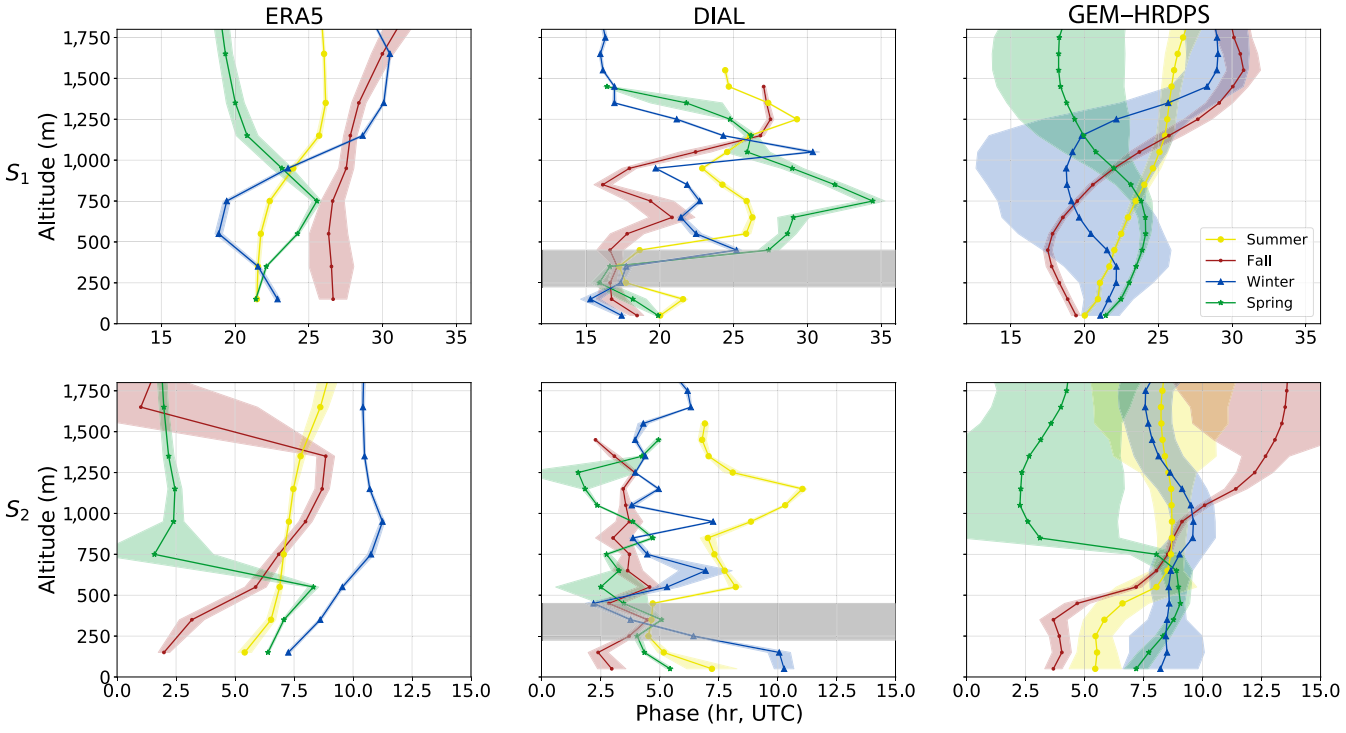

FIGURE 4 Same as Figure 3, but for the diurnal cycle's phase. Phases are calculated as the time, in hours, of the first maximum. The S_1 phases are continued past 24 hr (and S_2 past 12 hr) to better visualize the change in phase. [Colour figure can be viewed at wileyonlinelibrary.com]

1477870x, 0, Downloaded from https://rmets.onlinelibrary.wiley.com/doi/10.1002/qj.4520 by German Meteorological Service, Wiley Online Library on [06/08/2023]. See the Terms and Conditions (https://onlinelibrary.wiley.com/terms-and-conditions) on Wiley Online Library for rules of use; OA articles are governed by the applicable Creative Commons License

exhibit a clear seasonal cycle with summer amplitudes between 0.1 and 0.2 g·kg^{-1} and winter amplitudes between 0.003 and 0.02 g·kg^{-1}. The standard deviation of the GEM amplitudes is larger than the DIAL's, particularly in the winter and spring when the water vapour concentrations are low. The winter S_1 and S_2, as well as the spring S_2, shading continues out of bounds of the figure due to the log scaling. The shading encompasses values close to zero, which are not shown here. ERA5 S_1 amplitudes are also correlated with the season; however, the spring amplitudes are larger than the fall amplitudes in the first 600 m. The standard deviations of the ERA5 amplitudes are also small, except in the fall. The larger standard deviation in amplitude in the fall may explain why ERA5's diurnal cycle does not resemble the DIAL or GEM's cycle in Figure 2. Both numerical products' S_2 amplitudes are an order of magnitude smaller than their S_1 amplitudes. Unlike the DIAL S_2 components, the ERA5 and GEM S_2 components are more correlated with season, with the exception of the first 400 m.

The phases of the individual diurnal cycle components are shown in Figure 4. Here, we show the phases as the hour (UTC) at which the first maximum occurs. For visualization purposes, the S_1 phases are continued past 24 hr. The GEM fall S_2 phase is also wrapped around 12 hr. The phase of the DIAL S_1 component is subject to a solar cycle in the first 200 m. In the summer, the maximum occurs at 2000 UTC and gradually moves towards earlier in the day at 1600 UTC in the winter. However, the S_2 component does not seem to be subject to a solar cycle at those altitudes and is, for the most part, constant with altitude. Above 500 m, almost all seasons shift by 5–10 hr from their surface phases. Above 1 km, all seasons either reach a constant phase with altitude (summer and fall) or shift back towards their surface values (winter and spring). The standard deviation of the DIAL phases are less than an hour in both S_1 and S_2, suggesting that the DIAL solutions are also stable in phase.

ERA5 phases are shifted with respect to the DIAL's. The summer, winter, and spring S_1 phases are 2-4 hr later than the DIAL phases, and the ERA5 fall is completely out of phase with the DIAL by 15 hr, resulting in the disagreement seen in Figure 2. Unlike the DIAL S_2 components, which are constant with altitude, ERA5 S_2 phases start earlier than the DIAL at lower altitudes and gradually shift to later in the day. Although they are biased with respect to the DIAL, the solutions are relatively stable with standard deviations around 1 hr.

GEM produces S_1 phases that are close to the DIAL's in the first few hundred metres in the summer and fall, but the winter and spring maxima occur later by 3–4 hr. Although the GEM S_1 phases do shift towards later hours at higher altitudes, as the DIAL does, the GEM solutions shift more smoothly, and sometimes they reach the same phase as the DIAL at a higher altitude. For example, in the summer, the DIAL abruptly changes phase from 1700 UTC to 0200 UTC at 500 m, but the GEM S_1 cycle gradually shifts the phase to later in the day/early morning and reaches the 0200 UTC phase at 1,000 m. The GEM S_1 is out of phase with the DIAL in two altitude regions: above 1 km in the winter and between 800 and 1,200 m in the spring. The sizes of the GEM phase standard deviations are sensitive to low water vapour concentrations. In the spring, summer, and fall (larger water-vapour concentrations) the standard deviation values are small, but they gradually increase with altitude as the water vapour concentrations decrease. In the winter, when concentrations are small, the standard deviation values are larger (3–5 hr) throughout the profile.

The GEM S_2 phases shift smoothly with altitude and are not constant like the DIAL S_2 phases, with the exception of the winter. Whereas the summer GEM S_2 phase agrees well with the DIAL, the winter is shifted by roughly 3 hr for almost the entire altitude range. The GEM spring S_2 agrees well above 750 m but is shifted below by 2 hr. Finally, the fall S_2 agrees well below 500 m but quickly shifts out of phase above 500 m.

4.3 | Total column diurnal cycles

The total column diurnal cycles in ERA5 and GEM were examined and evaluated against the GPS IWV measurements. As with the height-resolved cycles, the GPS, ERA5, and GEM IWV diurnal cycles are calculated by fitting Equation (3) to their respective IWV time series. Figure 5 shows the diurnal cycles for ERA5, the GPS, and GEM, by season, and Tables 2 and 3 list the corresponding amplitudes and phases of the S_1 and S_2 fitted components. As with the height-resolved cycles, the comparison starts at 1200 UTC.

In some seasons, a discontinuity can be seen in each of the models (2400 UTC for ERA5, 36/1200 UTC for GEM) and the GPS time series (29/0500 UTC). The mechanism of the GPS discontinuity is discussed in Section 2. ERA5 is also known to have discontinuities in the surface temperature and humidity diurnal cycles (Hersbach *et al.,* 2018a), which may also contribute to the ERA5 discontinuity in IWV. The different timing of the discontinuities is due to averaging the hourly bins and the times that were chosen to complete each dataset's analysis. The GPS measurement solutions are calculated over 24 hr in local time (Hicks-Jalali *et al.,* 2021) and then shifted back to UTC, producing a discontinuity at 29/0500 UTC (since Iqaluit is at UTC−0500). The discontinuity in the GEM cycles at 36/1200 UTC is due to starting the time series

1477870x, 0, Downloaded from https://rmets.onlinelibrary.wiley.com/doi/10.1002/qj.4520 by German Meteorological Service, Wiley Online Library on [06/08/2023]. See the Terms and Conditions (https://onlinelibrary.wiley.com/terms-and-conditions) on Wiley Online Library for rules of use; OA articles are governed by the applicable Creative Commons License

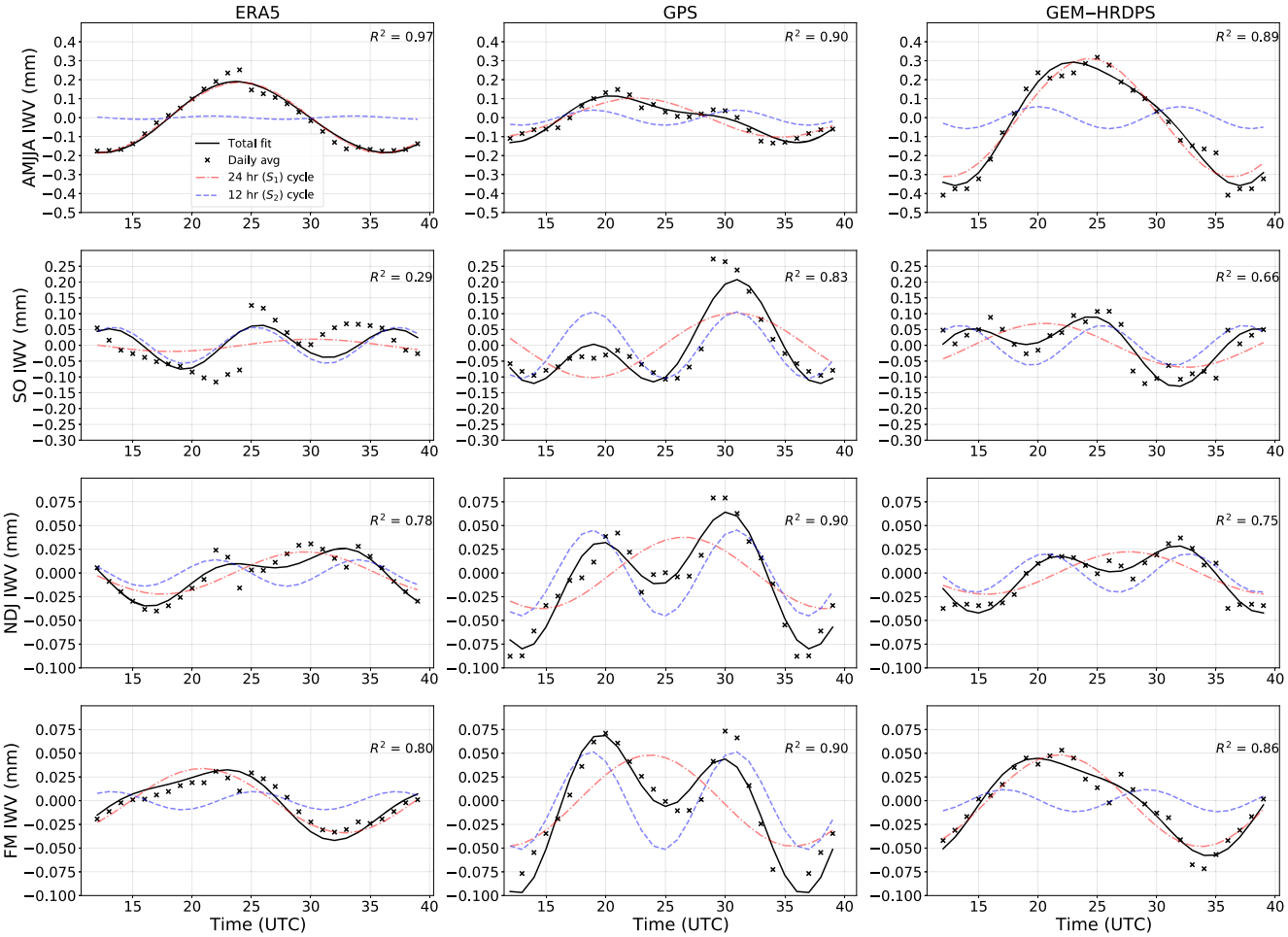

FIGURE 5 Diurnal integrated water vapour (IWV) cycles and solutions for European Centre for Medium-Range Weather Forecasts Reanalysis v5 (ERA5; column 1), Global Positioning System (GPS; column 2), and Global Environmental Multiscale–High Resolution Deterministic Prediction System (GEM–HRDPS; column 3). The total fit ($S_1 + S_2$; black, solid), S_1 component (red, dot-dashed), S_2 component (blue, dashed), and the hourly measurements (black ×) are shown. Note the change in scale of the *y*-axis for each row. Rows are divided seasonally, with row 1 as the summer analysis (April–August, AMJJA), row 2 for fall (September–October, SO), row 3 for winter (November–January, NJD), and row 4 for the spring (February–March, FM). [Colour figure can be viewed at wileyonlinelibrary.com]

hourly averaging at 1200 UTC. The ERA5 hourly average is calculated from 0000 to 2400 UTC, hence the discontinuity occurs at 2400 UTC. Though these discontinuities are unfortunate, and they can be mitigated with different averaging techniques (in the case of the GPS), they are known artefacts of the datasets and cannot be completely removed.

When comparing the GPS and GEM IWV cycles, we must also consider the slight interdependence of the results. As GEM assimilates GPS ZTDs and the GPS IWV values are derived from the same measurements, the GEM and GPS IWV values may have some dependence. However, the degree to which the GPS and GEM cycles disagree across all seasons suggests that the dependence on each other is minimal and does not affect the results significantly. Additionally, the GEM and ERA5 (where no GPS values are assimilated) IWV results show very similar behaviour, suggesting that the GPS influence on the GEM IWV cycle is minimal.

During the summer, all three datasets' diurnal cycles are primarily driven by the S_1 component. Though the GPS cycle is primarily driven by the S_1 component, it has a significant contribution from the S_2 component as well. The extended peak is due to the constructive interference between the two components and their slight offset in phase. The ERA5 summer IWV total cycle is almost entirely driven by the S_1 component, which is slightly larger in amplitude than the GPS by 0.08 mm (Table 2). The S_1 component also peaks 2 hr later than the GPS S_1 component (Table 3). GEM also produces a larger S_1 component (0.31 mm) relative to the S_2, although its S_2 cycle is of similar magnitude to the GPS's (0.06 mm). GEM produces both S_1 and S_2 maxima roughly 1 hr later than the GPS observations.

1477870x, 0, Downloaded from https://rmets.onlinelibrary.wiley.com/doi/10.1002/qj.4520 by German Meteorological Service, Wiley Online Library on [06/08/2023]. See the Terms and Conditions (https://onlinelibrary.wiley.com/terms-and-conditions) on Wiley Online Library for rules of use; OA articles are governed by the applicable Creative Commons License

TABLE 2 Integrated water vapour (IWV) amplitudes (by diurnal component) for the European Centre for Medium-Range Weather Forecasts Reanalysis v5 (ERA5), the Global Positioning System (GPS), and the Global Environmental Multiscale–High Resolution Deterministic Prediction System (GEM–HRDPS) for each season.

		IWV amplitudes (mm)			
		Summer (AMJJA)	Fall (SO)	Winter (NDJ)	Spring (FM)
S_1	GPS	0.10	0.10	0.04	0.05
	ERA5	0.18	0.02	0.02	0.03
	GEM–HRDPS	0.31	0.07	0.02	0.05
S_2	GPS	0.04	0.11	0.04	0.05
	ERA5	0.01	0.05	0.01	0.01
	GEM–HRDPS	0.06	0.06	0.02	0.01

Note: AMJJA: April–August; SO: September–October; NDJ: November–January; FM: February–March.

TABLE 3 Integrated water vapour (IWV) phases (by diurnal component) for the European Centre for Medium-Range Weather Forecasts Reanalysis v5 (ERA5), the Global Positioning System (GPS), and the Global Environmental Multiscale–High Resolution Deterministic Prediction System (GEM–HRDPS) for each season. Phases are calculated as the time, in hours, of the first maximum in UTC time.

		IWV phases (hr)			
		Summer (AMJJA)	Fall (SO)	Winter (NDJ)	Spring (FM)
S_1	GPS	22.59	6.83	2.54	23.69
	ERA5	0.01	6.17	5.49	20.85
	GEM–HRDPS	0.34	20.52	3.63	21.73
S_2	GPS	6.92	6.93	6.85	6.76
	ERA5	9.67	1.36	9.96	1.20
	GEM–HRDPS	7.98	1.42	8.67	5.19

Note: AMJJA: April–August; SO: September–October; NDJ: November–January; FM: February–March.

The fall cycles have a larger contribution from the S_2 component in both numerical products and in the GPS. The GPS S_2 amplitude increases to the same magnitude as the S_1, and the superposition of the two components creates the largest maximum at 31/0700 UTC. The GPS and ERA5 measurements have larger discontinuities in the fall due to the rapid decrease in water vapour per day (Hicks-Jalali *et al.*, 2021). ERA5 has almost no S_1 component during the fall, and though the GEM S_1 amplitude is larger than ERA5's it is still smaller than the GPS amplitude. The ERA5 and GPS S_1 components peak earlier than the GEM S_1 maximum by 14 hr. The ERA5 and GEM S_2 components are half that of the GPS S_2 amplitude and they are both off-phase by more than 5 hr with respect to the GPS.

Winter IWV cycles are equally influenced by both components. Both ERA5 and GEM have similar cycles in amplitude (0.02 mm for S_1 and S_2) and phase (0400–0500 UTC for S_1 and 0800–0900 UTC for S_2). On the other hand, the GPS cycles are slightly larger, as was observed in the DIAL's height-resolved cycles. The ERA5 S_1 maxima occurs 3 hr later than the GPS maxima, whereas the GEM S_1 maxima occurs 1 hr later than the GPS maxima. The GPS S_2 maxima occur earlier than either ERA5 or GEM by about 2–3 hr. In the spring, both numerical products reproduce the increase in the S_1 component; however, only GEM reproduces it at the same magnitude as the GPS (0.05 mm). ERA5 produces the S_1 peak 3 hr earlier than the GPS, and 2 hr earlier than GEM. The most significant difference between the numerical products and the GPS in this season is that the magnitude of the S_2 component is five times larger for the GPS than the models. The ERA5 S_2 component is 5 hr 30 min earlier than the GPS component, whereas GEM is 1 hr 30 min earlier.

4.4 | Lead-time dependence

In this section we present the stability of the diurnal water-vapour cycle with respect to the starting point of the time series for the ERA5 and DIAL measurements. For the GEM model, we analyse the sensitivity of the water-vapour cycle as the lead time of the forecast solution is gradually increased (whereas ERA5 and the DIAL do not have lead times). To examine the stability of the diurnal cycle solutions, we shifted the starting points of ERA5's and DIAL's time series for each hour such that the time series were calculated by taking the 24 hr from 0000 UTC, 0100 UTC, 0200 UTC, up to 2400 UTC and recalculating the diurnal cycle solution for each shifted time series. In GEM's case we always consider forecasts with initialization time at 0600 UTC; the first calculation will use lead times from initialization through the 24 hr forecast, then the 1 hr forecast lead time through the 25 hr forecast lead time, and so on until the 24 hr forecast through the 48 hr forecast. When discussing GEM we will use the term "lead time", whereas we will use "starting point of the time series" with ERA5, the DIAL, and the GPS, as they do not have lead times.

We analyse the effects of changing the starting point of the time series (for ERA5 and the DIAL) and gradually increasing the lead time (for GEM) on the biases of the amplitude and phase of the water vapour diurnal cycle, as fitted by Equation (3). We found no systematic features in the bias for a specific lead time, indicating that no particular lead time in GEM was better than the others for the

1477870x, 0, Downloaded from https://rmets.onlinelibrary.wiley.com/doi/10.1002/qj.4520 by German Meteorological Service, Wiley Online Library on [06/08/2023]. See the Terms and Conditions (https://onlinelibrary.wiley.com/terms-and-conditions) on Wiley Online Library for rules of use; OA articles are governed by the applicable Creative Commons License

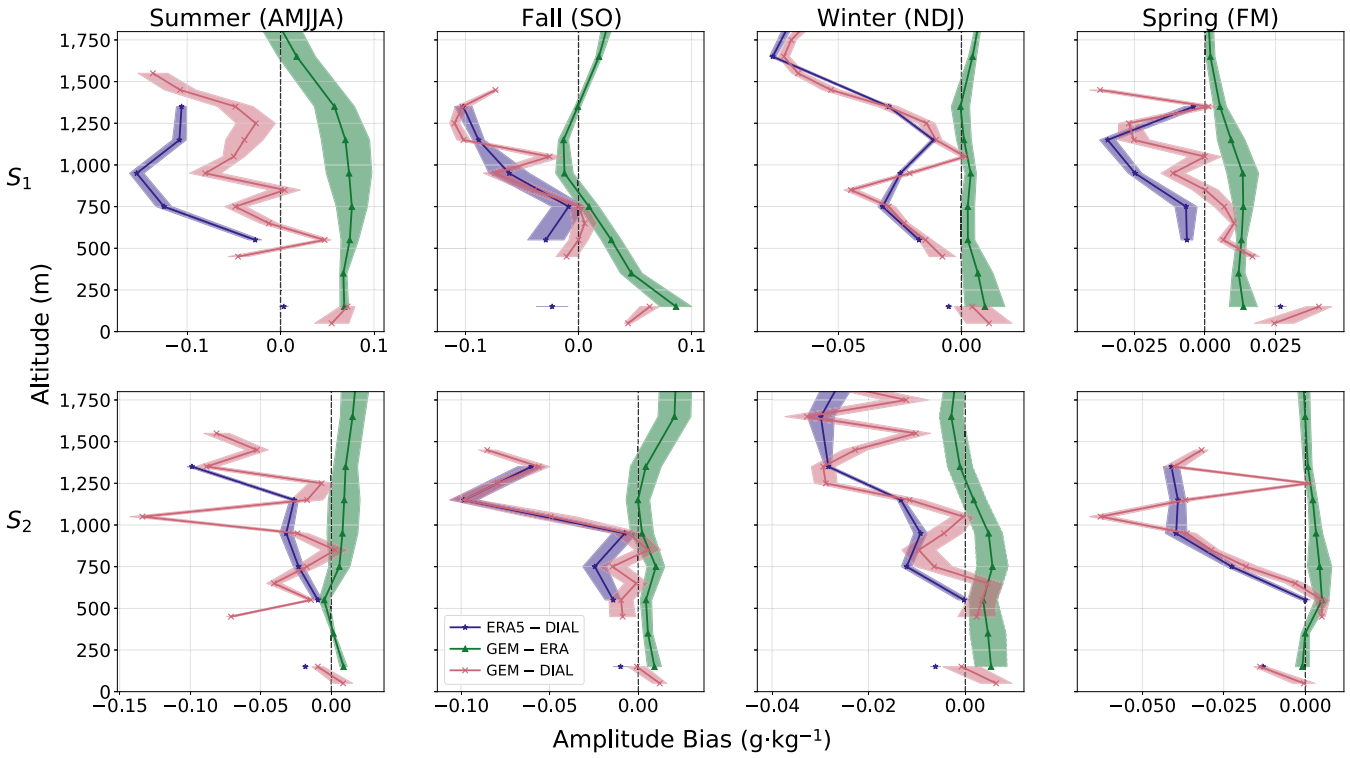

FIGURE 6 Height-resolved average amplitude biases (solid line) and the standard deviation of the bias (shaded area) between each dataset separated by the season and diurnal cycle component. Biases are represented as follows: ERA5-DIAL in blue stars, GEM-ERA5 in green triangles, and GEM-DIAL with red x's. [Colour figure can be viewed at wileyonlinelibrary.com]

height-resolved cycles and that the DIAL and ERA5 time series were not sensitive to the starting point of the time series.

The average bias of the diurnal cycle amplitude, averaged over the 24 solutions found when changing the starting point of the time series (and lead time for GEM), and the corresponding standard deviations are shown in Figure 6. The standard deviations of the solutions were presented in Figures 3 and 4. Small standard deviations in the bias indicate a stable solution that does not vary significantly with lead time/starting point of the time series. The points between 250 m and 450 m have been removed in the bias calculations with respect to the DIAL due to the known internal cycle in the DIAL.

GEM S_1 amplitudes are consistently larger than the DIAL's in the first 200 m by 0.02–0.05 g·kg^{-1} for every season. As the altitude increases, GEM S_1 bias is increasingly negative compared to the DIAL's S_1 amplitude. This is because the DIAL's S_1 amplitude tends to increase with altitude, while the GEM's either decrease or remain the same. The standard deviation of the GEM – DIAL bias is small, between 0.02 and 0.003 g·kg^{-1} (5–45% of the corresponding seasonal diurnal amplitude) depending on the season and altitude. ERA5 – DIAL S_1 amplitude biases vary by season in the first 200 m (blue solid line in Figure 6) but overall agree well with the DIAL. ERA5 – DIAL S_1 amplitude bias behaves similarly to the GEM – DIAL bias (decreasing with altitude) and is more negative than the GEM – DIAL bias in summer and spring. The standard deviation of the ERA5 – DIAL bias is also small, on the order of 0.01–0.02 g·kg^{-1}. The region between 450 m and 1 km is where the best agreement of the numerical products with the DIAL occurs, particularly for GEM. There is worse agreement close to the surface and above the planetary boundary layer.

In the summer and spring, GEM S_1 amplitudes are consistently larger than ERA5's by 0.05 g·kg^{-1}, whereas amplitudes are similar in the winter. In the fall, GEM – ERA5 amplitude bias is positive for lower altitudes and then it becomes neutral above 700 m. The standard deviation of the bias is generally larger between GEM and ERA5 than between the numerical products and the DIAL.

Whereas the S_1 amplitude biases between the numerical products and the DIAL varied with season, the S_2 amplitude biases did not. As seen in Figure 3, the ERA5 and GEM S_2 amplitudes are smaller than the DIAL S_2 amplitudes, and their difference increases with altitude. The best agreement between the DIAL and the models is in the first 200 m, where the amplitudes are similar. However, this is because the S_2 amplitude is almost negligible at

1477870x, 0, Downloaded from https://rmets.onlinelibrary.wiley.com/doi/10.1002/qj.4520 by German Meteorological Service, Wiley Online Library on [06/08/2023]. See the Terms and Conditions (https://onlinelibrary.wiley.com/terms-and-conditions) on Wiley Online Library for rules of use; OA articles are governed by the applicable Creative Commons License

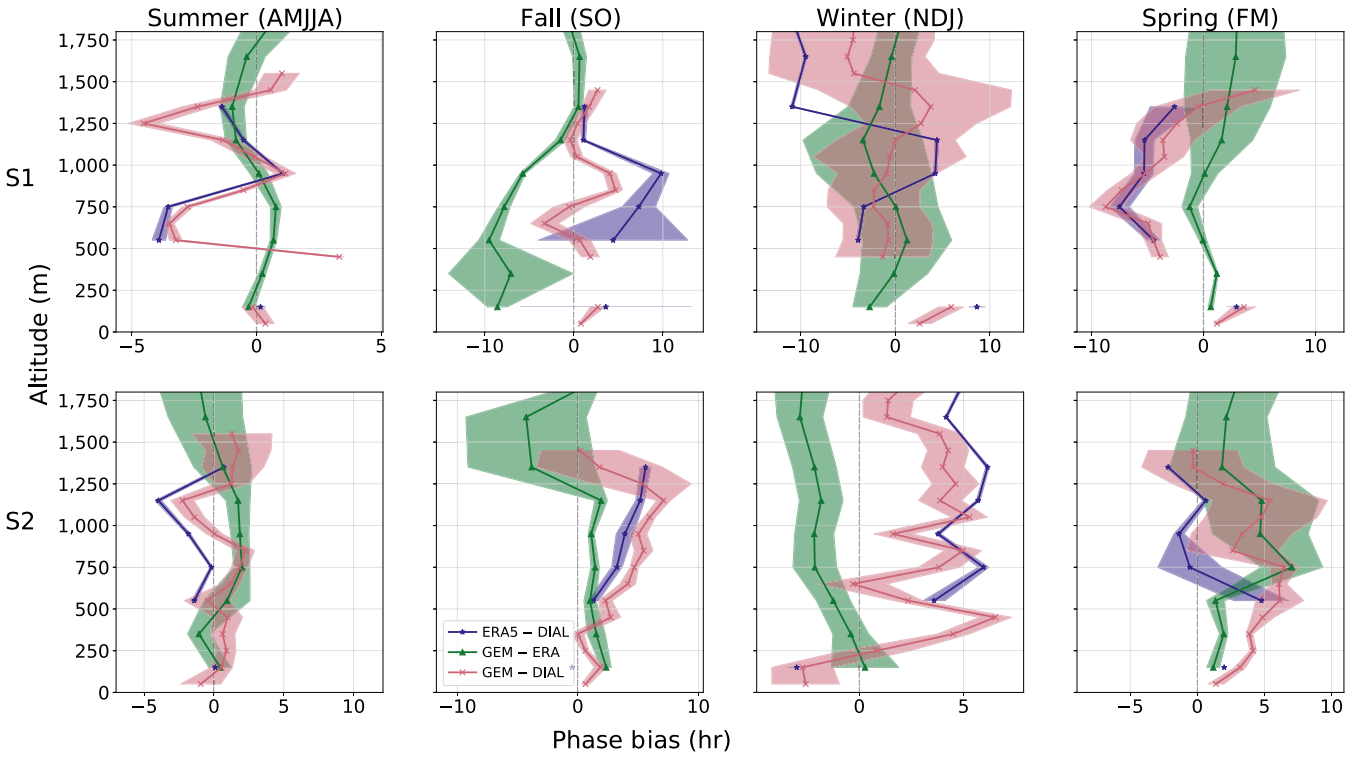

FIGURE 7 Same as Figure 6, except for diurnal cycle phase. [Colour figure can be viewed at wileyonlinelibrary.com]

those altitudes. As the S_2 amplitude increases with altitude and becomes more prominent above 1 km, the discrepancy between the numerical products and the DIAL worsens and the amplitude differences between them increases. The standard deviation of the S_2 amplitude biases is fairly constant with season and altitude, around 0.005 g·kg^{-1}. The GEM − ERA5 S_2 amplitude bias is almost neutral (slightly positive), for all seasons and altitudes, and again exhibits a larger standard deviation than the bias of the numerical products against the DIAL. The larger standard deviation of the GEM − ERA5 bias is due to the larger standard deviation of the GEM solutions compared with ERA5. Their almost zero bias between the two numerical products suggests that the models both have a difficult time reproducing the S_2 component.

Figure 7 is calculated in the same manner as Figure 6, but for the phases. The phase bias is calculated in hours. Similar to the amplitude biases, for S_1 we see the best agreement between the DIAL and GEM in the first 200 m, with biases ranging from 0 to 5 hr and standard deviations of the bias on the order of 0.5 to 1 hr. The GEM − DIAL S_1 phase solutions are most stable in the summer and fall, with very small standard deviations, whereas they exhibit a large spread in winter (same as the GEM − ERA5 S_1 bias). The GEM − DIAL biases switch with altitude between positive and negative values in summer and fall, whereas spring is dominated by a negative bias (GEM maximum occurs earlier than in the DIAL). Winter S_1 GEM phase solutions were highly sensitive to lead time. This was likely due to the low concentrations of water vapour, which made fitting difficult. Additionally, the models have difficulty replicating the diurnal cycle phase above 1 km in the winter (as seen in Figure 7), which likely contributes to the higher standard deviations between the GEM and DIAL above 1 km. The ERA5 − DIAL winter phase biases, on the other hand, were not sensitive to the time-series shift.

The S_2 phases show the best agreement between DIAL and the numerical products in summer and the worst agreement in winter. In the shoulder seasons (spring and fall) the S_2 phase bias is positive for all comparisons, indicating that the ERA5 peak occurs later than the DIAL (blue), that the GEM peak occurs later than in ERA5 (green), and that the GEM peak occurs later than in the DIAL (red). The standard deviations of the S_2 GEM − DIAL and GEM − ERA5 biases increase with altitude, except in the winter, likely due to the smaller water vapour concentrations above the boundary layer.

Similar to the height-resolved cycles, we evaluated model IWV diurnal cycles biases for their dependence on lead time and starting hour of the time series. Results for the amplitude biases are presented in Table 4 for each season. In the summer, the GEM model has a significant positive bias with respect to both the GPS and ERA5, whereas the ERA5 − GPS bias is small. The larger positive bias from

1477870x, 0, Downloaded from https://rmets.onlinelibrary.wiley.com/doi/10.1002/qj.4520 by German Meteorological Service, Wiley Online Library on [06/08/2023]. See the Terms and Conditions (https://onlinelibrary.wiley.com/terms-and-conditions) on Wiley Online Library for rules of use; OA articles are governed by the applicable Creative Commons License

TABLE 4 Average Integrated water vapour (IWV) amplitude bias and standard deviation with changing lead time.

		IWV amplitude bias ± *SD* (mm)			
		Summer (AMJJA)	**Fall (SO)**	**Winter (NDJ)**	**Spring (FM)**
S_1	ERA5 – GPS	0.083 ± 0.008	−0.042 ± 0.025	−0.014 ± 0.001	−0.017 ± 0.004
	GEM – GPS	0.198 ± 0.062	−0.038 ± 0.015	−0.018 ± 0.003	0.003 ± 0.003
	GEM – ERA5	0.115 ± 0.055	0.004 ± 0.031	−0.004 ± 0.004	0.020 ± 0.005
S_2	ERA5 – GPS	−0.033 ± 0.003	−0.057 ± 0.010	−0.030 ± 0.001	−0.044 ± 0.002
	GEM – GPS	0.006 ± 0.018	−0.053 ± 0.011	−0.030 ± 0.005	−0.043 ± 0.003
	GEM – ERA5	0.039 ± 0.018	0.004 ± 0.010	0.000 ± 0.005	0.001 ± 0.004

Note: AMJJA: April–August; SO: September–October; NDJ: November–January; FM: February–March.

TABLE 5 Average phase bias and standard deviation with changing lead time in hours UTC time.

		IWV phase bias ± *SD* (hr)			
		Summer (AMJJA)	**Fall (SO)**	**Winter (NDJ)**	**Spring (FM)**
S_1	ERA5 – GPS	1.197 ± 0.154	−1.179 ± 1.673	2.804 ± 0.183	−2.518 ± 0.383
	GEM – GPS	0.801 ± 0.584	-8.835 ± 1.709	2.521 ± 2.766	−0.903 ± 0.960
	GEM – ERA5	−0.396 ± 0.446	−2.856 ± 7.198	−0.283 ± 2.942	1.615 ± 0.804
S_2	ERA5-GPS	−0.208 ± 4.376	−6.039 ± 0.451	3.117 ± 0.093	−5.856 ± 0.454
	GEM – GPS	0.034 ± 3.525	−5.884 ± 0.419	2.036 ± 0.575	−0.711 ± 3.273
	GEM – ERA5	0.242 ± 4.095	0.155 ± 0.148	−1.081 ± 0.633	5.145 ± 3.234

Note: AMJJA: April–August; SO: September–October; NDJ: November–January; FM: February–March.

GEM is likely due to an assimilation effect, which also contributes to the larger standard deviations and sensitivity to lead time. In the fall, the GEM bias with respect to GPS improves, but the standard deviation remains slightly high. In the fall, the ERA5 and GEM biases with respect to the GPS are similar in magnitude and indicate an underprediction of the amplitude of the numerical products.

In the winter, both ERA5 and GEM had average S_1 amplitude biases lower than the GPS and both biases were stable with respect to the diurnal cycle initial hour. GEM and ERA5 solutions were similar with respect to each other, with a small average bias of −0.004 mm. In the spring, ERA5 had an overall negative bias with respect to the GPS, and the solution had little dependence on the starting point of the time series. GEM agreed well with the GPS with an equally small standard deviation in the bias. As expected, GEM – ERA5 S_1 amplitude exhibits a positive bias of 0.02 mm.

The S_2 IWV amplitude biases for the summer behave differently than in the other seasons. In the summer, ERA5 underestimate the amplitude with respect to GPS (by 0.033 mm), whereas GEM slightly overestimates it (by 0.006 mm). As expected, the difference between GEM and ERA is of 0.039 mm. The spread of the biases when comparing GEM with either GPS or ERA5 is significantly larger than when comparing GPS versus ERA5, suggesting once again (as for S_1) a stronger sensitivity to the GEM lead time than to the GPS and ERA5 initial hour for the time-series fit. In fall, winter, and spring, both GEM and ERA5 underestimate the S_2 amplitude (by 0.05 mm, 0.03 mm, and 0.04 mm respectively) with respect to the GPS. As expected, the GEM – ERA5 bias is almost null in these seasons. The spread for these seasons shows stability in the results.

The average IWV biases in phase and their standard deviations are presented in Table 5. With the exception of the fall GEM solution, ERA5 and GEM in general reproduce the S_1 phase within 1–3 hr of the GPS S_1 phase. The standard deviation of the biases varies somewhat more with the season, being stable in the summer (0.15–0.58 hr) and less stable in the fall and winter. Though the ERA5 and the GPS S_1 phases agree well in the fall, the GEM S_1 arrives almost 9 hr earlier. The high standard deviation in the fall biases is likely caused by the larger discontinuity in the ERA5 and GPS solutions and the steep decrease in water vapour over the season. In the winter, ERA5 and GEM exhibit similar average phase biases, but GEM's variation in the bias is much larger due to the large variability in the specific humidity height-resolved winter solutions. However, the spring GEM bias (−0.9 hr) and variability in

1477870x, 0, Downloaded from https://rmets.onlinelibrary.wiley.com/doi/10.1002/qj.4520 by German Meteorological Service, Wiley Online Library on [06/08/2023]. See the Terms and Conditions (https://onlinelibrary.wiley.com/terms-and-conditions) on Wiley Online Library for rules of use; OA articles are governed by the applicable Creative Commons License

the bias (−0.96 hr) improve as the water vapour concentrations increase.

The S_2 phase biases and their stability vary more with season compared with the S_1 phase solutions. In the summer, both ERA5 and GEM have small average phase biases with respect to the GPS, but their standard deviations are large (4 hr). The S_2 IWV amplitudes are at least half the size of the S_1 amplitudes in the summer. Their effect on the overall cycle is minimal; therefore, they are more sensitive to changes in the starting point of the time series. The opposite occurs in the fall, where both the GEM and ERA5 S_2 components have a large bias (−6 hr) yet small standard deviation (0.4 hr), suggesting that their solutions are stable with respect to the GPS and consistent across all lead times. In the winter, both ERA5 and GEM have similar S_2 phase biases with respect to the GPS, but the standard deviation of their biases are relatively small. Lastly, the spring average S_2 phase bias improved for GEM (−0.711 hr) but increased for ERA5 (−5.856 hr). However, the GEM − GPS and GEM − ERA5 biases are less stable, likely due to the larger standard deviation in the higher altitudes of the GEM height-resolved cycles.

5 | SUMMARY AND DISCUSSION

5.1 | Connecting the height-resolved and IWV cycles

Both ERA5 and GEM numerical products agreed well with the DIAL and GPS seasonally. As expected, the summer months had the largest average water vapour concentrations (around 3 g·kg^{-1}), and spring was the driest season (between 0.5 and 0.7 g·kg^{-1}). Both models also accurately reproduced (with respect to the DIAL, Figure 1) the variability in the water-vapour profiles at all altitudes. The GEM and ERA5 seasonal IWV averages all agreed with the GPS averages within their respective standard deviations, except for a small 1 mm bias in the winter and spring. This bias is likely caused by the assimilation of radiosondes, which are known to have a dry bias in cold temperatures (Miloshevich *et al.,* 2009; Dirksen *et al.,* 2014). The average specific humidity profiles in this study are consistent with others conducted at similar latitudes (Serreze *et al.,* 1995; Jakobson and Vihma, 2010; Graham *et al.,* 2019).

Graham *et al.* (2019) compared ERA5 with 27 independent radiosonde measurements over the Greenland Sea and showed that ERA5 was consistently within ±0.15 g·kg^{-1} of the radiosondes, with the sign depending on the altitude. We observed slight biases of less than 0.25 g·kg^{-1} between the DIAL and both numerical products, mostly due to sampling differences. Mariani *et al.* (2021) evaluated GEM at Iqaluit using measurements from September 2018 to August 2019 and found a mean bias of −0.16±0.02 g·kg^{-1} (GEM − DIAL) for the entire year. In this study, we expanded the analysis in Mariani *et al.* (2021) to include measurements from January to June 2020 and found a similar mean bias of −0.13 ± 0.44 g·kg^{-1}. Note that in our study we use the average bias plus/minus the standard deviation of the bias, whereas Mariani *et al.* (2021) used the standard deviation of the mean. Mariani *et al.* (2021) also found that GEM has a slight moist bias around 150 m.

ERA5 and GEM produced mixed results when evaluated at the diurnal time-scale (Figure 2), varying with season and altitude. In general, the DIAL and ERA5 diurnal-cycle solutions were stable and showed very little variation when the starting point of their time series was changed (Figures 3,4,6, and 7). The GEM model solutions were more sensitive to decreasing water vapour concentrations, with low standard deviations in their solutions below 1 km and in the summer and fall, but the variability increased in the winter and spring and above 1 km for all seasons.

In the summer, ERA5 is able to reproduce the overall phase of the diurnal specific-humidity cycle, but it lacks the structure and amplitudes observed by the DIAL measurements. The structure observed in the total diurnal cycle in the DIAL is due to the influence of the S_2 component (Hicks-Jalali *et al.*, 2021), which is an order of magnitude smaller in ERA5 than in the DIAL. The ERA5 summer S_1 amplitudes are smaller by 0.1 g·kg^{-1} for all altitudes. Thus, the combination of smaller diurnal amplitudes in both S_1 and S_2 and the lack of variability in phase in both components creates a smaller ERA5 IWV diurnal cycle with a broader maximum compared with the DIAL. Similar to ERA5, GEM lacks the structure and variability of the DIAL cycle in the summer, but it is better able to reproduce the magnitude of the diurnal height-resolved cycle than ERA5 is. However, GEM produces larger S_1 amplitudes than DIAL by 0.06 g·kg^{-1} at 150 m. Additionally, above 1 km the GEM S_2 component is an order of magnitude smaller than the DIAL S_2 amplitude and is out of phase; consequently, it does not reproduce the interaction between the S_1 and S_2 components to create the increase in total diurnal amplitude observed by the DIAL.

Hicks-Jalali *et al.* (2021) found that the DIAL's height-resolved and GPS's IWV diurnal cycles corroborated each other in phase, which we also find to be true in ERA5 and GEM and their corresponding IWV cycles. The summer ERA5 IWV cycle has a prominent S_1 component and almost no S_2 component. The ERA5 S_1 IWV component is also larger than the GPS S_1 component by 0.08 mm. The GEM total IWV diurnal cycle is also dominated by the S_1 component, although the S_2 component is of similar magnitude to the GPS S_2 amplitude. The

1477870x, 0, Downloaded from https://rmets.onlinelibrary.wiley.com/doi/10.1002/qj.4520 by German Meteorological Service, Wiley Online Library on [06/08/2023]. See the Terms and Conditions (https://onlinelibrary.wiley.com/terms-and-conditions) on Wiley Online Library for rules of use; OA articles are governed by the applicable Creative Commons License

lack of S_2 component in the ERA5 IWV diurnal cycle is consistent with the very small S_2 component present in the height-resolved cycles.

The larger S_1 amplitude in ERA5 suggests that ERA5 expects a larger diurnal cycle than what the GPS measures; however, the height-resolved diurnal cycles were smaller in amplitude than in the DIAL. One possibility for the discrepancy is the unfortunate coincidence that the ERA5 IWV cycle maximum occurs at the same time as the discontinuity in the ERA5 cycle; thus, this maximum may have been artificially increased. It is also possible that the DIAL amplitudes above 1 km are overestimated. The R^2 values in that region are low; however, Hicks-Jalali *et al.* (2021) found that the summer amplitudes at those altitudes were in agreement with Jakobson *et al.* (2014). Hicks-Jalali *et al.* (2021) also compared the summer GPS cycles with the Jakobson *et al.* (2009) GPS diurnal cycles and found that although the Iqaluit GPS diurnal cycles were on the low end of the distribution they still agreed with the Jakobson *et al.* (2009) observations. The bias in ERA5's IWV amplitude could be related to an overestimation of evapotranspiration at Iqaluit.

The GEM IWV S_1 amplitude also exhibited a large average bias (0.2 mm) with respect to the GPS S_1 component (Table 4). This positive bias in the IWV S_1 component in GEM is corroborated by the corresponding positive bias in the height-resolved S_1 component in the first 200 m in the DIAL observations and is likely due to the assimilation of the GPS ZTD measurements at the 0600 UTC initialization time. During the summer, the assimilation effect was larger than the other seasons and persisted to the sixth hour lead time. At later lead times the bias between GEM and the GPS decreased (later lead times exhibited decreased bias between GEM and GPS; not shown). The large change in the bias with lead time was apparent in the larger standard deviation of the GEM − GPS bias shown in Table 4. The larger amplitudes in the first few hundred metres of the height-resolved cycles are likely affected by the ZTD assimilation as well, because the hydrometric component of the ZTD is dominated by boundary-layer water vapour. Another possibility is that the GEM model also overestimates the evapotranspiration rate for Iqaluit.

In the fall, ERA5 has almost no diurnal cycle present due to extremely small amplitudes in both S_1 and S_2 components at all altitudes. The DIAL total diurnal cycle is driven by the S_1 component for the first 1 km. Above 1 km the DIAL has a large diurnal maximum that is created via the superposition of the S_1 and S_2 components. Though GEM correctly reproduces the S_1 phase below 1 km, the S_2 component phase is too early and is an order of magnitude smaller than the DIAL S_2 amplitude, such that it cannot create the same intense maximum above 1 km.

The fall GPS IWV cycles are clearly influenced by the S_2 component; however, the DIAL height-resolved cycles are primarily driven by the S_1 component up to 1 km. We can examine how the height-resolved cycles influence the total IWV cycle by looking at the similarities in phase between the two cycles. The GPS IWV maxima correspond to the maximum from 100 m to 1 km in the DIAL and the 30/0600 UTC maximum above 1 km. Both the GEM S_1 and S_2 IWV amplitudes are smaller in magnitude than the GPS IWV amplitudes, thus creating a smaller total cycle than the GPS cycle. The GEM IWV total cycle is mostly characterized by the increased S_2 amplitude (0.05 mm). As with the DIAL and GPS cycles, the GEM S_2 IWV phase corresponds with the GEM S_2 phase at 1,400 m, with a slight offset of 1 hr. The phase differences between the GEM components and the DIAL components above 1 km appear to have a significant effect on their respective total IWV diurnal cycles. The GEM IWV maxima of the total diurnal cycle are shifted by 3 hr with respect to the GPS due to the phase shift of the GEM S_2 component above 1 km, and the GEM IWV cycle has a deep minimum at 32/0800 UTC that is not present in the GPS cycle. Thus, the phases of the height-resolved cycle components impact the behaviour of the IWV cycle.

It is difficult to resolve a diurnal cycle in the DIAL and numerical products in the winter and spring months due to the lower water vapour content. Nevertheless, as discussed in Hicks-Jalali *et al.* (2021), the agreement in phase between the DIAL and GPS and in the surface amplitudes from the WMO surface station provide confidence in the DIAL results. In the winter, ERA5 has almost no diurnal cycle present for the entire altitude range, and GEM has a small amplitude of 0.03 $g \cdot kg^{-1}$ at 150 m (a small positive bias of 0.02 $g \cdot kg^{-1}$ with the DIAL). GEM and ERA5 are not able to reproduce phase shifts and the S_2 component above 500 m that are observed by the DIAL. Most notably, the DIAL observes a large maximum at 1700 UTC above 1 km created by the superposition of the two components and increased amplitude of the S_2 component. Though both GEM and ERA5 reproduce increases in magnitude at those altitudes, they are 12–14 hr out of phase with the DIAL. The GEM and ERA5 S_1 and S_2 components are shifted with respect to each other, resulting in a total extended maximum instead of a defined peak.

As observed in the fall, the winter IWV cycles seem to reflect the height-resolved cycles around or above 1 km. The GPS cycle is clearly defined by the S_2 component, with maxima that correspond to the DIAL S_2 phases between 900 and 1,250 m. ERA5's IWV S_2 phase is consistent with its height-resolved S_2 phase around 1,200 m, as are the GEM cycles. The superpositioning of the DIAL height-resolved cycles above 1 km results

1477870x, 0, Downloaded from https://rmets.onlinelibrary.wiley.com/doi/10.1002/qj.4520 by German Meteorological Service, Wiley Online Library on [06/08/2023]. See the Terms and Conditions (https://onlinelibrary.wiley.com/terms-and-conditions) on Wiley Online Library for rules of use; OA articles are governed by the applicable Creative Commons License

in stronger maximums in the GPS IWV cycles. In GEM and ERA5, the S_1 and S_2 components are out of phase and have smaller S_2 amplitudes, such that they get more of an extended IWV maximum with smaller S_2 peaks.

In the spring, the ERA5 and GEM S_1 components at 150 m are in phase with the surface cycle and agree well in magnitude; however, the GEM S_1 amplitude has a slight positive bias of 0.025 g·kg^{-1} around 50 m. Though the DIAL S_2 amplitudes increase in altitude, the GEM and ERA5 height-resolved mixing ratio amplitudes decrease, thus limiting the IWV S_2 component. Both ERA5 and GEM do not produce the S_2 component during the spring or the winter. The lack of the S_2 component in spring and winter, and in the summer as well, suggests that there is a process (or several) that is not being well represented in the models.

The results of the fall, winter, and spring cycles indicate that the IWV cycles are heavily influenced by the water vapour above 1 km, and less so by the water vapour close to the surface. Jakobson *et al.* (2014) also found that 60% of the diurnal variability over land was driven by the layers between 800 and 900 hPa, which corresponds to approximately 500–2,000 m at Iqaluit. The behaviour observed here agrees with their results and is easily observed in the fall and winter when the S_1 amplitude is small enough to allow the S_2 component to dominate.

Louf *et al.* (2015) examined height-resolved diurnal water vapour cycles in Africa using a microwave radiometer. Their fig. 6 depicts the height-resolved cycles and IWV cycles of the total column, a column below 1,400 m and another above 1,400 m. The column above 1,400 m has more water vapour, and their fig. 6 indicates that the total cycle can be determined by the summation of the two layers. In their fig. 6b, the total cycle is a summation of the two layers but retains the overall behaviour of the layer above 1,400 m. This would suggest that the diurnal IWV cycle may strongly depend on the 800–900 hPa region; however, more investigation is required on a global scale to verify if this is true elsewhere.

5.2 | Possible causes of the differences between the model and observation diurnal cycles

This is the first time that the GEM diurnal water-vapour cycles have been evaluated, whereas a few recent papers have evaluated the IWV diurnal cycles in ERA5 in the Tropics. Lees *et al.* (2021) evaluated ERA5 diurnal IWV cycles around the south Indian Ocean basin. They also found that that the ERA5 IWV diurnal amplitudes were underestimated with respect to the GPS measurements. Xue *et al.* (2020) analysed the diurnal cycles of upper tropospheric humidity between ±60° latitude using brightness temperatures from satellite-based imagers. They found that all five reanalysis datasets (including ERA5) had smaller diurnal amplitudes than the observations and that the phase of the maximum humidity lagged behind the observations by 3 hr. Our results corroborate the findings from both papers, that both ERA5 IWV and height-resolved amplitudes are smaller than those observed.

There are several factors that may be influencing the differences between the two models themselves and between the models and observations. The first major difference is their resolutions. ERA5's horizontal resolution is significantly coarser than the resolution of GEM. Other studies have shown that models with higher resolutions are more successful at reproducing diurnal cycles of precipitation and convection. Sato *et al.* (2009) tested three different resolutions of the Nonhydrostatic Icosahedral Atmospheric Model between 14 km, 7 km, and 3 km across the globe between ±30° latitude to evaluate the model's precipitation diurnal cycle. They found that the 3 km model outperformed the lower resolution models over both land and the ocean.

Milbrandt *et al.* (2016) suggests that at higher model resolutions there is less need for deep convection parametrization; however, more attention must be paid to the microphysics at kilometre scales. GEM does have a deep convection scheme (Kain and Fritsch, 1990) in addition to the predicted particle properties microsphysics scheme. ERA5 also has a deep convection parametrization scheme that did improve the diurnal cycle of precipitation and convection in the Tropics (Bechtold *et al.*, 2014). However, the Bechtold *et al.* (2014) model is dependent on the level of convective available potential energy, which may not work as well for sites at higher latitudes where there is little to no convection. We used vertical wind measurements from the wind lidar to examine convection in Iqaluit during the course of this study to verify this; however, we could not detect a diurnal signal in the vertical wind during any season, suggesting that convection is not very strong at Iqaluit. ERA5 also made improvements to their microsphysics scheme (Ahlgrimm and Forbes, 2014), and though it did improve top-of-atmosphere short-wave radiation bias in the model globally, it did not improve the negative bias in top-of-atmosphere short-wave radiation around Iqaluit. Future work is required to evaluate how well Arctic clouds are reproduced in GEM and ERA5 at Iqaluit.

The ratio of land to water in each grid point is another significant difference between the two models. The Iqaluit ERA5 pixel is 50% split between land and water, whereas

1477870x, 0, Downloaded from https://rmets.onlinelibrary.wiley.com/doi/10.1002/qj.4520 by German Meteorological Service, Wiley Online Library on [06/08/2023]. See the Terms and Conditions (https://onlinelibrary.wiley.com/terms-and-conditions) on Wiley Online Library for rules of use; OA articles are governed by the applicable Creative Commons License

the GEM grid point is 80% land and 20% water. Iqaluit is far enough north that sea breezes are not much of an influence on the diurnal cycle and can only occur during July and August Mariani *et al.* (2018). However, a lack of sea-surface temperature information and the influence of the ice in Frobisher Bay may not be completely accounted for in ERA5, resulting in low diurnal amplitudes in the fall and winter.

GEM exhibited a small but consistent positive bias in the near-surface bins with respect to the DIAL, particularly in the summer months. Land-surface processes (such as evapotranspiration) and other complex processes (such as water vapour flux from snow) may need to be examined in further detail to explain this bias. The type of vegetation assumed for Iqaluit and the seasonal soil moisture are also variables that would contribute to the evapotranspiration estimates and should be evaluated in future analyses. There have been fewer opportunities to evaluate the evapotranspiration process for vegetation found in Iqaluit and the tundra environment in GEM in comparison with lower latitude Canada, and as such it may not be accurately represented. Both GEM and ERA5 assimilate soil moisture measurements, either from satellites or from ground-based in-situ measurements (Albergel *et al.,* 2012; De Rosnay *et al.,* 2013; Carrera *et al.,* 2015). However, in GEM's case, the soil moisture measurements are only assimilated in grid points with a land/water ratio higher than 90% and are not assimilated if snow, frozen soil, or precipitation is present in the nature run (Carrera *et al.,* 2015). Therefore, soil moisture is likely not assimilated for the Iqaluit grid point in this study, which could be causing some of the bias in the near-surface cycles. GEM and ERA5 may also be assuming that the Iqaluit soil is not frozen in the summer, and though the top layers of soil will melt in July and August, the lower layers will remain frozen, which would impact the amount of moisture available to evaporate in the summer.

Given Iqaluit's location and the lack of observations available to assimilate in this region, models are generally forced to rely on assimilating satellite measurements. However, satellite-based instrument measurements are generally limited in temporal coverage of a specific location. Additionally, satellite-based instrument humidity measurements usually have low vertical resolution (several hundred metres to kilometres) and either have no measurements or have high uncertainties in the boundary layer. ERA5 significantly increased its assimilated observations worldwide; however, Hersbach *et al.* (2020) did not differentiate the number of measurements by latitude. GEM is able to assimilate more radiosondes and aircraft measurements than previous versions (Buehner *et al.,* 2015), but since those measurements do not have high temporal resolution they would have less of an effect on the diurnal cycle. Additionally, ERA5 does not assimilate ZTD, whereas GEM does for every run. Assimilating the GPS measurements improved the IWV forecasts over North America (Macpherson *et al.,* 2008; Buehner *et al.,* 2015). Assimilating the ZTDs, which are mostly influenced by the water vapour in the first few kilometres, may help constrain the boundary-layer humidity in GEM. Nevertheless, it is clear that the models would benefit from additional higher temporal and vertical resolution humidity measurements in the Arctic.

6 | CONCLUSIONS

Diurnal cycles are one of the most challenging components of numerical weather prediction and climate models to reproduce due to their complexity and dependence on numerous processes. High-frequency thermodynamic measurements in the Arctic are difficult to maintain for extended periods of time due to the harsh environment and large expense, making evaluations of numerical weather and climate models difficult. In this article, we have evaluated the seasonal and diurnal water vapour behaviour in the ECMWF ERA5 model and the ECCC GEM NWP model against a preproduction DIAL system and ground-based GPS observations taken at the ECCC Iqaluit supersite.

Both ERA5 and GEM were able to reproduce the seasonal averages and the standard deviation of the water vapour observed by the DIAL and the GPS. However, although the numerical products perform well on the seasonal scale, the diurnal cycle remains challenging, particularly when resolved by height. Near-surface, summer height-resolved, and summer IWV cycles showed the best agreement between both numerical products and the observations. Winter and spring exhibited the worst agreement in the height-resolved cycles due to low water vapour concentrations. Though GEM was able to reproduce the fall cycle below 1 km, it struggled above; ERA5 was unable to resolve a height-resolved or IWV cycle in the fall.

Both numerical products have trouble reproducing the diurnal cycle above 1 km, particularly the S_2 component. Other studies have shown that ERA5, although it has improved over ERA-Interim, still produces diurnal amplitudes that are smaller than those observed. We showed that, in Iqaluit, ERA5 S_1 amplitudes agreed with the DIAL in the summer and spring close to the surface but were smaller above 500 m by 0.1 $g \cdot kg^{-1}$. The ERA5 S_2 amplitudes were significantly smaller than those of the DIAL and GPS at all altitudes and were generally out of phase. The lack of an S_2 component significantly affected the numerical product IWV cycles, such that their amplitudes

1477870x, 0, Downloaded from https://rmets.onlinelibrary.wiley.com/doi/10.1002/qj.4520 by German Meteorological Service, Wiley Online Library on [06/08/2023]. See the Terms and Conditions (https://onlinelibrary.wiley.com/terms-and-conditions) on Wiley Online Library for rules of use; OA articles are governed by the applicable Creative Commons License

were also smaller than the GPS IWV amplitudes except in the summer, when their amplitudes were larger than the GPS'. ERA5's bias in phase and amplitude was constant with shifting the time series starting point, so we can conclude that the solution was mostly unaffected by changing the starting point of the time series.

The GEM diurnal cycles were closer to the DIAL and GPS than the ERA5 cycles. This was likely primarily due to GEM's higher resolution (2.5 km), which has been demonstrated to improve diurnal cycles in previous studies, but also potentially due to the grid-point tile water/land composition. GEM also assimilates GPS measurements, which provide additional water vapour information in the lower troposphere and boundary layer, whereas ERA5 does not. GEM is also designed specifically for Canada. The GEM S_1 component agreed well with the DIAL below 1 km and was mostly in phase with the DIAL results below 1 km. However, above 1 km the GEM S_1 amplitudes were typically smaller than the DIAL S_1 amplitudes. Like ERA5, GEM had trouble reproducing the S_2 component in both the height-resolved profiles and consequently in the IWV cycles as well. The DIAL measurements revealed an S_2 amplitude that increases with altitude, which neither ERA5 nor the GEM could reproduce. The GEM bias with respect to the DIAL and the GPS was fairly constant, with minimal dependence on lead time. Higher altitudes were subject to larger variation, presumably because the amplitudes were smaller at those altitudes and the average water vapour content was much smaller (typically 1 $g \cdot kg^{-1}$ less than at the surface).

This article has shown that the S_2 component is a critical process in Iqaluit's diurnal cycle. The inability to reproduce the S_2 component in the diurnal cycle profiles has important consequences on the accuracy (magnitude and phase) of the models' net (sum) diurnal cycle, possibly affecting other atmospheric processes, such as precipitation. We found that the IWV diurnal cycle is highly dependent on the diurnal water vapour cycle between 500 m and 2,000 m. In this region, the influence of the S_2 component becomes visible due to its increase in amplitude and its constructive interference with the 24 hr component. If the S_2 component is incorrect, it affects the IWV cycles such that their amplitudes are either too small or they are shifted in phase with respect to the GPS. Total column and humidity profiles are crucial components of the radiative transfer equations that govern NWP. Incorrect timing of the diurnal component can have consequences on the timing of precipitation, cloud formation, or convective processes. Finding the drivers of the S_2 component is an important next step in improving diurnal cycles in NWP. Future work will involve investigating measurements of pressure, precipitation, soil moisture, cloud, and surface turbulent flux diurnal cycles at Iqaluit and comparing them with ERA5 and GEM to hopefully determine which processes are the source of the discrepancies.

AUTHOR CONTRIBUTIONS

Shannon Hicks-Jalali: conceptualization; data curation; formal analysis; investigation; methodology; software; visualization; writing – original draft; writing – review and editing. **Zen Mariani:** data curation; funding acquisition; project administration; resources; software; supervision; validation; writing – review and editing. **Barbara Casati:** data curation; resources; validation; writing – review and editing. **Sylvie Leroyer:** data curation; resources; validation; writing – review and editing. **François Lemay:** data curation; resources; software. **Robert W. Crawford:** data curation; resources; software.

ACKNOWLEDGEMENTS

Special thanks to Sorin Pinzariu, Michael Harwood, Robert Reed, Reno Sit, Jason Iwachow, Michael Travis, and Daniel Coulombe for their help with instrumentation at the Iqaluit site and to Dr William Burrows and Dr Jason Milbrandt for their help and advice on working with the GEM output.

CONFLICT OF INTEREST STATEMENT

The instrument manufacturer had no role in the design of the study, in the collection, analyses, or interpretation of data used to perform the instrument or model comparisons, in the writing of the manuscript, or in the decision to publish the results.

ORCID

Shannon Hicks-Jalali https://orcid.org/0000-0001-6682-4406

REFERENCES

Ahlgrimm, M. and Forbes, R. (2014) Improving the representation of low clouds and drizzle in the ECMWF model based on arm observations from the Azores. *Monthly Weather Review*, 142, 668–685.

Albergel, C., Balsamo, G., Rosnay, P.D. and Muñoz-sabater, J. (2012) A bare ground evaporation revision in the ECMWF land-surface scheme: Evaluation of its impact using ground soil moisture and satellite microwave data. *Hydrology and Earth System Sciences*, 16(10), 3607–3620. https://doi.org/10.5194/hess-16-3607-2012.

Bechtold, P., Kohler, M., Jung, T., Doblas-Reyes, F., Leutbecher, M., Rodwell, M.J., Vitart, F. and Balsamo, G. (2008) Advances in simulating atmospheric variability with the ECMWF model: from synoptic to decadal time-scales. *Quarterly Journal of the Royal Meteorological Society*, 134, 1337–1351 http://www.kemkes.go.id.

Bechtold, P., Semane, N., Lopez, P., Chaboureau, J.P., Beljaars, A. and Bormann, N. (2014) Representing equilibrium and

1477870x, 0, Downloaded from https://rmets.onlinelibrary.wiley.com/doi/10.1002/qj.4520 by German Meteorological Service, Wiley Online Library on [06/08/2023]. See the Terms and Conditions (https://onlinelibrary.wiley.com/terms-and-conditions) on Wiley Online Library for rules of use; OA articles are governed by the applicable Creative Commons License

nonequilibrium convection in large-scale models. *Journal of the Atmospheric Sciences*, 71, 734–753.

Bevis, M., Businger, S., Chiswell, S., Herring, T.A., Anthes, R.A., Rocken, C. and Water, R.H. (1994) GPS meteorology: mapping zenith wet delays onto precipitable water. *Journal of Applied Meteorology*, 33, 379–386.

Bevis, M., Businger, S., Herring, T.A., Rocken, C., Anthes, R.A. and Ware, R.H. (1992) GPS meteorology: remote sensing of atmospheric water vapor using the global positioning system. *Journal of Geophysical Research*, 97, 787–801.

Blewitt, G., Hammond, W. and Kreemer, C. (2018) Harnessing the GPS data explosion for interdisciplinary science. *Eos*. https://eos.org/science-updates/harnessing-the-gps-data-explosion-for-interdisciplinary-science

Bock, O., Guichard, F., Janicot, S., Lafore, J.P., Bouin, M.N. and Sultan, B. (2007) Multiscale analysis of precipitable water vapor over Africa from GPS data and ECMWF analyses. *Geophysical Research Letters*, 34, 1–6.

Bouma, H.R. and Stoew, B. (2001) GPS observations of daily variations in the atmospheric water vapor content. *Physics and Chemistry of the Earth, Part A: Solid Earth and Geodesy*, 26, 389–392.

Buehner, M., McTaggart-Cowan, R., Beaulne, A., Charette, C., Garand, L., Heilliette, S., Lapalme, E., Laroche, S., Macpherson, S.R., Morneau, J. and Zadra, A. (2015) Implementation of deterministic weather forecasting systems based on ensemble–Variational data assimilation at Environment Canada. Part I: the global system. *Monthly Weather Review*, 143, 2532–2559.

Caron, J.-F., Milewski, T., Buehner, M., Fillion, L., Reszka, M., Macpherson, S. and St-James, J. (2015) Implementation of deterministic weather forecasting systems based on ensemble –Variational data assimilation at Environment Canada. Part II: the regional system. *Monthly Weather Review*, 143, 2560–2580.

Carrera, M.L., Bélair, S. and Bilodeau, B. (2015) The Canadian land data assimilation system (CaLDAS): description and synthetic evaluation study. *Journal of Hydrometeorology*, 16, 1293–1314.

Chepfer, H., Brogniez, H. and Noel, V. (2019) Diurnal variations of cloud and relative humidity profiles across the tropics. *Scientific Reports*, 1–9. https://doi.org/10.1038/s41598-019-52437-6.

Chung, E., Soden, B.J., Sohn, B.J. and Schmetz, J. (2013) An assessment of the diurnal variation of upper tropospheric humidity in reanalysis data sets. *Journal of Geophysical Research Atmospheres*, 118, 3425–3430.

Côté, J., Gravel, S., Méthot, A., Patoine, A., Roch, M. and Staniforth, A. (1998) The operational CMC-MRB global environmental multiscale (GEM) model. Part I: design considerations and formulation. *Monthly Weather Review*, 126, 1373–1395.

Dai, A. and Trenberth, K.E. (2004) The diurnal cycle and its depiction in the community climate system model. *Journal of Climate*, 17, 930–951.

Dai, A., Wang, J., Ware, R.H. and Van Hove, T. (2002) Diurnal variation in water vapor over North America and its implications for sampling errors in radiosonde humidity. *Journal of Geophysical Research*, 107, 11.

De Rosnay, P., Drusch, M., Vasiljevic, D., Balsamo, G., Albergel, C. and Isaksen, L. (2013) A simplified extended Kalman filter for the global operational soil moisture analysis at ECMWF. *Quarterly Journal of the Royal Meteorological Society*, 139, 1199–1213.

Dirksen, R.J., Sommer, M., Immler, F.J., Hurst, D.F., Kivi, R. and Vömel, H. (2014) Reference quality upper-air measurements: GRUAN data processing for the Vaisala RS92 radiosonde. *Atmospheric Measurement Techniques*, 7, 4463–4490.

Brockman, E. (2020) EUREF Repro2 contribution of Swisstopo E. In: Jones, J., Guerova, G., Dousa, J., Dick, G., de Haan, S., Pottiaux, E., Bock, O., Pacione, R. and van Malderen, R. (Eds.) *Advanced GNSS Tropospheric Products for Monitoring Severe Weather Events and Climate*, 1st edition. Cham, Switzerland: Springer Nature Switzerland, pp. 158–162.

Emardson, T.R., Elgered, G. and Johansson, J.M. (1998) Three months of continuous monitoring of atmospheric water vapor with a network of global positioning system receivers. *Journal of Geophysical Research Atmospheres*, 103, 1807–1820.

Gaffard, C., Li, Z., Harrison, D., Lehtinen, R. and Roininen, R. (2021) *Evaluation of a Prototype Broadband Water-Vapour Profiling Differential Absorption Lidar at Cardington*. Atmosphere: UK, p. 12.

Galisteo, J.P.O.D., Cachorro, V., Toledano, C., Torres, B. and Laulainen, N. (2011) Diurnal cycle of precipitable water vapor over Spain. *Quarterly Journal of the Royal Meteorological Society*, 137, 948–958.

Graham, R.M., Hudson, S.R. and Maturilli, M. (2019) Improved performance of ERA5 in Arctic gateway relative to four global atmospheric reanalyses geophysical research letters. *Geophysical Research Letters*, 46, 6138–6147.

Haefele, A., Hocke, K., Kämpfer, N., Keckhut, P., Marchand, M., Bekki, S., Morel, B., Egorova, T. and Rozanov, E. (2008) Diurnal changes in middle atmospheric H_2O and O_3: observations in the alpine region and climate models. *Journal of Geophysical Research Atmospheres*, 113, 1–13.

Hersbach, H., Bell, B., Berrisford, P., Biavati, G., Horányi, A., Muñoz Sabater, J., Nicolas, J., Peubey, C., Radu, R., Rozum, I., Schepers, D., Simmons, A., Soci, C., Dee, D. and Thépaut, J.-N. (2018a) ERA5 hourly data on pressure levels from 1979 to present.

Hersbach, H., Bell, B., Berrisford, P., Biavati, G., Horányi, A., Muñoz Sabater, J., Nicolas, J., Peubey, C., Radu, R., Rozum, I., Schepers, D., Simmons, A., Soci, C., Dee, D. and Thépaut, J.-N. (2018b) ERA5 hourly data on single levels from 1979 to present.

Hersbach, H., Bell, B., Berrisford, P., Hirahara, S., Horányi, A., Munoz-Sabater, J., Nicolas, J., Peubey, C., Radu, R., Schepers, D., Simmons, A., Soci, C., Abdalla, S., Abellan, X., Balsamo, G., Bechtold, P., Biavati, G., Bidlot, J., Bonavita, M., De Chiara, G., Dahlgren, P., Dee, D., Diamantakis, M., Dragani, R., Flemming, J., Forbes, R., Fuentes, M., Geer, A., Haimberger, L., Healy, S., Hogan, R.J., Holm, E., Janisková, H.M., Keeley, S., Laloyaux, P., Lopez, P., Cristina, L., Radnoti, G., de Rosnay, P., Rozum, I., Vamborg, F., Villaume, S. and Thépaut, J.-N. (2020) The ERA5 global reanalysis. *Quarterly Journal of the Royal Meteorological Society*, 146, 1999–2049.

Hicks-Jalali, S., Mariani, Z. and Crawford, R.W. (2021) DIAL and GNSS observations of the diurnal water-vapour cycle above Iqaluit, Nunavut. *Quarterly Journal of the Royal Meteorological Society*, 147, 1–23.

Hocke, K., Navas-Guzmán, F., Moreira, L., Bernet, L. and Mätzler, C. (2017) Diurnal cycle in atmospheric water over Switzerland. *Remote Sensing*, 9, 909 http://www.mdpi.com/2072-4292/9/9/909.

1477870x, 0, Downloaded from https://rmets.onlinelibrary.wiley.com/doi/10.1002/qj.4520 by German Meteorological Service, Wiley Online Library on [06/08/2023]. See the Terms and Conditions (https://onlinelibrary.wiley.com/terms-and-conditions) on Wiley Online Library for rules of use; OA articles are governed by the applicable Creative Commons License

Jakobson, E., Keernik, H., Luhamaa, A. and Ohvril, H. (2014) Diurnal variability of water vapour in the Baltic Sea region according to NCEP-CFSR and BaltAn65+ reanalyses. *Oceanologia*, 56, 191–204. https://doi.org/10.5697/oc.56-2.191.

Jakobson, E., Ohvril, H. and Elgered, G. (2009) Diurnal variability of precipitable water in the Baltic region, impact on transmittance of the direct solar radiation. *Boreal Environment Research*, 14, 45–55.

Jakobson, E. and Vihma, T. (2010) Atmospheric moisture budget in the Arctic based on the ERA-40 reanalysis. *International Journal of Climatology*, 30, 2175–2194.

Joe, P., Melo, S., Burrows, W.R., Casati, B., Crawford, R.W., Deghan, A., Gascon, G., Mariani, Z., Milbrandt, J. and Strawbridge, K. (2020) The Canadian arctic weather science project: introduction to the Iqaluit site. *Bulletin of the American Meteorological Society*, 101, E109–E128.

Jones, J., Guerova, G., Dousa, J., Dick, G., de Haan, S., Pottiaux, E., Bock, O., Pacione, R. and van Malderen, R. (Eds.). (2020) *Advanced GNSS Tropospheric Products for Monitoring Severe Weather Events and Climate*. Cham, Switzerland: Springer Nature Switzerland.

Kain, J.S. and Fritsch, J.M. (1990) A one-dimensional entraining/detraining plume model and its application in convective parameterization. *Journal of Atmospheric Sciences*, 47, 2784–2802.

Knuteson, R.O., Revercomb, H.E., Best, F.A., Ciganovich, N.C., Dedecker, R.G., Dirkx, T.P., Ellington, S.C., Feltz, W.F., Garcia, R.K., Howell, H.B., Smith, W.L., Short, J.F. and Tobin, D.C. (2004a) Atmospheric emitted radiance interferometer. Part I: instrument design. *Journal of Atmospheric and Oceanic Technology*, 21, 1763–1776.

Knuteson, R.O., Revercomb, H.E., Best, F.A., Ciganovich, N.C., Dedecker, R.G., Dirkx, T.P., Ellington, S.C., Feltz, W.F., Garcia, R.K., Howell, H.B., Smith, W.L., Short, J.F. and Tobin, D.C. (2004b) Atmospheric emitted radiance interferometer. Part II: instrument performance. *Journal of Atmospheric and Oceanic Technology*, 21, 1777–1789.

Lees, E., Bousquet, O., Roy, D. and de Bellevue, J.L. (2021) Analysis of diurnal to seasonal variability of integrated water vapour in the South Indian Ocean basin using ground-based GNSS and fifth-generation ECMWF reanalysis (ERA5) data. *Quarterly Journal of the Royal Meteorological Society*, 147, 229–248.

Louf, V., Pujol, O., Sauvageot, H. and Riédi, J. (2015) Seasonal and diurnal water vapour distribution in the Sahelian area from microwave radiometric profiling observations. *Quarterly Journal of the Royal Meteorological Society*, 141, 2643–2653.

Macpherson, S., Deblonde, G., Aparicio, J.M. and Casati, B. (2008) Impact of NOAA ground-based GPS observations on the Canadian regional. *Monthly Weather Review*, 136, 2727–2746.

Mariani, Z., Dehghan, A., Gascon, G., Joe, P., Hudak, D., Strawbridge, K. and Corriveau, J. (2018) Multi-instrument observations of prolonged stratified wind layers at Iqaluit, Nunavut. *Geophysical Research Letters*, 45, 1654–1660.

Mariani, Z., Hicks-Jalali, S., Strawbridge, K., Gwozdecky, J., Crawford, R.W., Casati, B., Lemay, F., Lehtinen, R. and Tuominen, P. (2021) Evaluation of Arctic water vapor profile observations from a differential absorption Lidar. *Remote Sensing*, 13, 1–21.

Mariani, Z., Stanton, N., Whiteway, J. and Lehtinen, R. (2020) Toronto water vapor Lidar inter-comparison campaign. *Remote Sensing*, 12, 1–12.

Milbrandt, J., Leroyer, S., Paquin-Ricard, D., Faucher, M., Zhang, S. and Jouan, C. (2018) *High Resolution Deterministic Prediction System (HRDPS). Tech. Rep. Canadian Meteorological Centre, Environment and Climate Change Canada*, Montreal, Canada.

Milbrandt, J.A., Belair, S., Faucher, M., Vallee, M., Carrera, M.L. and Glazer, A. (2016) The pan-Canadian high resolution (2.5 km) deterministic prediction system. *Weather and Forecasting*, 31, 1791–1816.

Milbrandt, J.A. and Morrison, H. (2016) Parameterization of cloud microphysics based on the prediction of bulk ice particle properties. Part III: introduction of multiple free categories. *Journal of the Atmospheric Sciences*, 73, 975–995.

Miloshevich, L.M., Vomel, H., Whiteman, D.N. and Leblanc, T. (2009) Accuracy assessment and correction of Vaisala RS92 radiosonde water vapor measurements. *Journal of Geophysical Research*, 114, 1–23.

Montmerle, T. (2020) *Statement of Guidance for High Resolution Numerical Weather Predition, Tech. rep*. World Meteorological Organization, Geneva, Switzerland. https://community.wmo.int/rolling-review-requirements-process.

Morrison, H. and Milbrandt, J.A. (2015) Parameterization of cloud microphysics based on the prediction of bulk ice particle properties. Part I: scheme description and idealized tests. *Journal of the Atmospheric Sciences*, 72, 287–311.

Newsom, R.K., Turner, D.D., Lehtinen, R., Münkel, C., Kallio, J. and Roininen, R. (2020) Evaluation of a compact broadband differential absorption LIDAR for routine water vapor profiling in the atmospheric boundary layer. *Journal of Atmospheric and Oceanic Technology*, 37, 47–65.

Sato, T., Miura, H., Satoh, M., Takayabu, Y.N. and Wang, Y. (2009) Diurnal cycle of precipitation in the tropics simulated in a global cloud-resolving model. *Journal of Climate*, 22, 4809–4826.

Semmler, T., Jacob, D., Schlünzen, K.H. and Podzun, R. (2005) The water and energy budget of the Arctic atmosphere. *Journal of Climate*, 18, 2515–2530.

Serreze, M.C., Barry, R.G. and Walsh, J.E. (1995) Atmospheric water vapor characteristics at 70°N. *Journal of Climate*, 8, 719–731.

Soden, B.J. (2000) The diurnal cycle of convection, clouds, and water vapor in the tropical upper troposphere. *Geophysical Research Letters*, 27, 2173–2176.

South, A.M., Povey, I.M. and Jones, R.L. (1998) Broadband LIDAR measurements of tropospheric water vapor profiles. *Journal of Geophysical Research Atmospheres*, 103, 31191–31202.

Stratton, R.A. and Stirling, A.J. (2012) Improving the diurnal cycle of convection in GCMs. *Quarterly Journal of the Royal Meteorological Society*, 138, 1121–1134.

Tian, B., Soden, B.J. and Wu, X. (2004) Diurnal cycle of convection, clouds, and water vapor in the tropical upper troposphere: satellites versus a general circulation model. *Journal of Geophysical Research*, 109, 1–16.

Wang, J., Dai, A., Carlson, D.J., Ware, R.H. and Liljegren, J.C. (2002) Diurnal variation in water vapor and liquid water profiles. In: *AMS Annual Meeting*. Orlando, FL, USA, pp. 3–6.

1477870x, 0, Downloaded from https://rmets.onlinelibrary.wiley.com/doi/10.1002/qj.4520 by German Meteorological Service, Wiley Online Library on [06/08/2023]. See the Terms and Conditions (https://onlinelibrary.wiley.com/terms-and-conditions) on Wiley Online Library for rules of use; OA articles are governed by the applicable Creative Commons License

https://ams.confex.com/ams/annual2002/techprogram/paper{_}27%917.htm.

World Meteorological Organization. (2016) *The Global Observing System for Climate: Implementation Needs* Tech. rep. Geneva, Switzlerand: World Meteorological Organization https://library.wmo.int/doc{_}num.php?explnum{_}id=3417.

Xue, Y., Li, J., Li, Z., Gunshor, M.M. and Schmit, T.J. (2020) Evaluation of the diurnal variation of upper tropospheric humidity in reanalysis using homogenized observed radiances from international geostationary weather satellites. *Remote Sensing*, 12, 1–14.

How to cite this article: Hicks-Jalali, S., Mariani, Z., Casati, B., Leroyer, S., Lemay, F. & Crawford, R.W. (2023) An assessment of Arctic diurnal water-vapour cycles in Canada's weather forecast model and ERA5. *Quarterly Journal of the Royal Meteorological Society*, 1–25. Available from: https://doi.org/10.1002/qj.4520

1477870x, 0, Downloaded from https://rmets.onlinelibrary.wiley.com/doi/10.1002/qj.4520 by German Meteorological Service, Wiley Online Library on [06/08/2023]. See the Terms and Conditions (https://onlinelibrary.wiley.com/terms-and-conditions) on Wiley Online Library for rules of use; OA articles are governed by the applicable Creative Commons License